NACA

RESEARCH MEMORANDUM

BASIC PRESSURE MEASUREMENTS ON A FUSELAGE AND A 45° SWEPTBACK WING-FUSELAGE COMBINATION AT TRANSONIC SPEEDS IN THE SLOTTED TEST SECTION OF THE LANGLEY 8-FOOT HIGH-SPEED TUNNEL

By Donald L. Loving and Claude V. Williams

Langley Aeronautical Laboratory
Langley Field, Va.

NATIONAL ADVISORY COMMITTEE
FOR AERONAUTICS

WASHINGTON

September 14, 1951

Classification cancelled (or changed to UNCLASSIFIED)

By Authority of NASA Tech Pub Announcement #1

(OFFICER AUTHORIZED TO CHANGE)

By [redacted] 28 Jan 58

[redacted]

GRADE OF OFFICER MAKING CHANGE)

24 Mar 61

DATE

NATIONAL ADVISORY COMMITTEE FOR AERONAUTICS

RESEARCH MEMORANDUM

BASIC PRESSURE MEASUREMENTS ON A FUSELAGE AND A 45° SWEPTBACK WING-FUSELAGE COMBINATION AT TRANSONIC SPEEDS IN THE SLOTTED TEST SECTION OF THE LANGLEY 8-FOOT HIGH-SPEED TUNNEL

By Donald L. Loving and Claude V. Williams

SUMMARY

The data presented herein are the first results of pressure measurements obtained on a fuselage and a 45° sweptback wing-fuselage combination at transonic speeds in the slotted test section of the Langley 8-foot high-speed tunnel. This test was part of a systematic investigation of varying amounts of sweepback on wings suitable for transonic flight. Pressure distributions were obtained at five spanwise stations on the wing and along six meridians on the fuselage.

The pressure diagrams for the wing were characterized by rearward shifts in center of pressure with increases in Mach number. Also large differences in upper and lower surface pressure coefficients in the region of the trailing edge were exhibited as the angle of attack was increased. As a result, large increases in load on the trailing edge were indicated for the high-angle-of-attack cases. Two discontinuities in the chordwise pressure diagrams were evident at Mach numbers on the order of 1.00. These discontinuities appeared to originate at the leading and trailing edges of the wing-fuselage juncture, extend outboard across the span, and merge near the wing tip.

The level of negative pressure coefficients remained relatively high on the rear portion of the fuselage upper surface throughout the angle of attack and Mach number range investigated.

Addition of the wing to the fuselage produced pronounced effects on the fuselage pressures in the region of the wing blanketed by the fuselage, resulting in considerable additions to the load carried by the fuselage. The fuselage pressures reflected the general chordwise

trends with increases in Mach number and angle of attack indicated by the inboard station of the wing.

INTRODUCTION

In the past, choking and blockage effects have been intimately associated with high-speed investigations in closed-throat wind tunnels. Installation of a slotted test section in the Langley 8-foot high-speed tunnel has made it possible to obtain aerodynamic data at Mach numbers through the speed of sound without the usual effects of choking and blockage. Recently pressure models of a fuselage and a wing-fuselage combination were investigated in this new type of test section at Mach numbers from 0.60 to 1.13. Data were obtained at angles of attack from 0° to 20° for most of the test Mach numbers, especially in the range from 0.94 to 1.13. These results fill the gap which has existed heretofore in wind-tunnel data through the transonic Mach number range and also extend the angle-of-attack range of previous investigations using the same model configurations. These previous investigations were made in a solid-nozzle test section of the Langley 8-foot high-speed tunnel and covered the angle-of-attack range from -2° to 14° at Mach numbers from 0.6 to 0.96 and from -2° to 6° at a supersonic Mach number of 1.2, as shown in reference 1. Force-test results for the same model and test conditions have been reported in reference 2.

The purpose of this paper is to make available the additional basic information obtained during the investigation at the earliest possible date after completion of the tests. Therefore, the analysis of the results is limited to a brief discussion only of the more significant indications obtained from the basic pressure distributions presented herein.

SYMBOLS

α	angle of attack of fuselage center line
b	wing span
M	Mach number
p_o	free-stream static pressure
p	local static pressure
P	pressure coefficient $\left(\frac{p - p_o}{q}\right)$

q	free-stream dynamic pressure $\left(\frac{1}{2}\rho V^2\right)$
ρ	mass density in undisturbed stream
V	velocity in undisturbed stream

APPARATUS

The investigation was conducted in the Langley 8-foot high-speed tunnel which is a dodecagonal, slotted-throat, single-return wind tunnel designed for continuous operation through the speed range up to a Mach number of 1.15. Calibrations of the flow in the slotted test section have indicated that very uniform flow exists throughout the speed range of the tunnel. Deviations from the free-stream Mach number, in the region occupied by the model, did not exceed a value of 0.008 in the speed range from $M = 1.11$ to 1.15. At Mach numbers below 1.02 the deviations did not exceed a value of 0.003. This degree of uniformity in the distribution of Mach number was considered quite satisfactory for model testing purposes in the subsonic, transonic, and supersonic speed ranges. Figure 1 presents Mach number distributions obtained along the center line of the slotted test section. Sufficient additional data have been obtained along the center line and off the center line to establish that the flow in the region of the model was equally as uniform off the center line as along the center line. Further investigation of the flow in the tunnel revealed that the angularity of flow was on the order of 0.10° and all data were obtained at corrected angles of attack to compensate for this angularity.

The wing of the configuration used in this investigation had 45° sweepback of the quarter-chord line, an aspect ratio of 4.0, a taper ratio of 0.6, and NACA 65A006 airfoil sections parallel to the air stream. The fuselage was designed with the ordinates of the general transonic fuselage and is the same fuselage used in the wing-fuselage combination. Dimensions of the model are presented in figure 2. Static-pressure orifices were divided among six meridians on the fuselage (A, B, C, D, E, and F) and five semispan stations on the wing parallel to the air stream (20 percent, 60 percent, and 95 percent on the left wing and 40 percent and 80 percent on the right wing). A detailed description of the model may be found in reference 1. The nose of the sting-mounted model was located 70 inches from the upstream apex of the test-section slots, measured along the tunnel center line (see fig. 3).

The angle of attack of the model was measured by the use of a cathetometer sighted at a line painted on the fuselage.

To keep the model located along the tunnel center line at the higher angles of attack, the sting configuration shown in figure 4 was used.

TESTS AND ACCURACY

The static-pressure data were obtained for the fuselage alone and a wing-fuselage combination. These basic pressure data were obtained for angles of attack of 0°, 4°, 8°, 12°, 18°, and 20° at Mach numbers of 0.60, 0.79, 0.89, 0.94, 0.97, 0.99, 1.02, 1.11, and 1.13. The rather odd Mach numbers for which data are presented are due to an original faulty calibration of the liquid (tetrabromoethane) used in the manometer tubes. The Mach numbers presented herein are the corrected values obtained from a recalibration of the manometer liquid.

An estimate of all the factors involved in obtaining the pressure coefficients indicated that the data are correct to within ±0.006. The accuracy of the cathetometer method of measuring the angle of attack was judged to be ±0.10°.

The slots in the test section of the Langley 8-foot high-speed tunnel were designed to eliminate tunnel-wall interference for nonlifting cases. Earlier tests in a circular slotted tunnel based on theory confirmed the theoretical predictions for nonlifting cases of zero-blockage interference and absence of choking (reference 3). Additional analytical studies have indicated that the effects of blockage were quite small for the lifting cases. Therefore, the data presented are considered free of tunnel-wall interference and no corrections have been applied. In the vicinity of the model, the magnitudes of the Mach number and pressure gradients were so small that no corrections due to these sources have been applied to the data.

Data have not been presented for Mach numbers between 1.02 and 1.11 to ensure that the results obtained were free of the effects of shock reflections from the tunnel walls.

RESULTS

The basic pressure data for the wing, obtained during tests of the wing-fuselage combination, are presented for five spanwise stations in figure 5. In this figure the circle symbols denote the upper surface and the square symbols denote the lower surface.

The basic pressure data for the fuselage alone and for the fuselage obtained during tests of the wing-fuselage combination are presented for

six fuselage meridians in figures 6 to 10. In all these figures the circle symbols designate the data obtained for the fuselage alone, and the square symbols designate the data for the fuselage with wing present.

DISCUSSION

Wing

All pressure data for the wing were obtained during the investigation of the wing-fuselage combination and hence were influenced by the presence of the fuselage. The distributions of pressure on the wing were characterized by rearward shifts in center of pressure as Mach number was increased and by increased loads on the trailing edge at the higher angles of attack.

0° angle of attack.- In figures 5(f), 5(h), 5(j), 5(l), 5(n), and 5(p), it is shown that as the Mach number was increased the regions of relatively high negative pressure coefficient shifted rearward all along the span. The greatest shift was noted for the 95-percent-semispan station. Here it is shown that at a Mach number of 0.94 (fig. 5(f)), the maximum value of negative pressure coefficient was located at approximately 20 percent of the chord, whereas at a Mach number of 1.13 (fig. 5(p)), the peak shifted rearward to the region of 70 percent of the chord.

4° and 8° angles of attack.- The pressure distributions presented for angles of attack of 4° and 8° as shown in figures 5(a), 5(f), 5(h), 5(j), 5(l), 5(n), and 5(p) are representative of the conditions existing throughout the linear portion of the lift-curve slope, with an angle of attack of 8° approximating the upper limit.

In contrast to the sharp leading-edge peaks in the pressure diagrams for an angle of attack of 4°, the leading-edge peaks at an angle of attack of 8° became increasingly broader toward the outboard regions of the wing. As a result, a slight rearward shift in center of pressure was indicated and an increase in loading occurred over the trailing edge of the outboard sections of the wing. When the Mach number was increased to 0.94 for these same angles of attack (fig. 5(f)), a second discontinuity in pressure-coefficient distribution followed by a rather poor pressure recovery was present on the upper surfaces. This discontinuity appeared to occur at the same chordwise location as the maximum negative pressure-coefficient peak noted for an angle of attack of 0°. The discontinuity seemed to originate at the juncture of the trailing edge of the wing with the surface of the fuselage. It crossed the wing at an angle somewhat less than the sweep of the wing and merged with the discontinuity on the forward portions of the wing. The

spanwise location at which the merger occurred appeared to move inboard with increase in angle of attack. As the Mach number was increased, the second discontinuity shifted rearward along the chord so that the chordwise extent of relatively high negative pressure coefficients increased, and the values of the peak negative pressure coefficient at the leading edge became more positive.

In the Mach number range between 0.99 and 1.02 (figs. 5(j) and 5(l), respectively), the level of pressures on the outboard portion of the wing revealed that a greater loading occurred on these outer stations than at the lower Mach numbers.

The pressure diagrams for Mach numbers up to 1.13 at these same angles of attack (fig. 5(p)), were similar to those measured at a Mach number of 0.99 (fig. 5(j)); however, the general level of the negative pressures on the upper surface was less than for a Mach number of 0.99. Generally, the induced pressure coefficients increase in a negative direction as the Mach number is increased towards the speed of sound and then decrease when the Mach number is increased beyond the speed of sound.

12°, 18°, and 20° angles of attack.- For angles of attack beyond the linear portion of the lift-curve slope and up to the region near maximum lift, $\alpha = 20°$, as shown in figures 5(b), 5(c), 5(d), 5(e), 5(g), 5(i), 5(k), 5(m), 5(o), and 5(q), the pressure diagrams were characteristic of separated flow over the wing. At these high angles of attack, the difference in the level of the pressure coefficients on the upper and lower surfaces of the wing indicated large loads on the wing trailing edge.

When the angle of attack was increased from 12° to 20° at Mach numbers from 0.6 to 0.94, as shown in figures 5(b), 5(c), 5(d), 5(e), and 5(g), nearly flat pressure distributions spread over most of the wing sections. As a result, the pressure coefficient at the 95-percent-chord location on the upper surface of the 40-percent-semispan station reached a value of approximately -0.73 at $\alpha = 20°$ and $M = 0.94$, (fig. 5(g)), and a large rearward shift in center of pressure was indicated. The levels of the pressure coefficients on the outboard sections were considerably less than the levels for the inboard stations indicating a greater load carried by the inboard stations than outboard. For example, the pressure coefficients on the inboard upper surface were about -0.8 compared to -0.4 outboard.

The level of negative pressure coefficients increased from -0.4 to -0.6 when Mach numbers on the order of 0.97, 0.99, and 1.02 were reached (figs. 5(i), 5(k), and 5(m), respectively). This increase indicated that the loss in load over the outboard stations was less severe than at the lower Mach numbers for these same angles of attack. At the same time the load on the trailing edge of the wing continued to increase. For example,

the differential in pressure coefficients between the upper and lower surfaces, at the 95-percent-chord station of the 40-percent-semispan station was approximately 95 percent of free-stream dynamic pressure q, at an angle of attack of 20° and a Mach number of 1.02 (fig. 5(m)).

The general forms of the pressure diagrams shown in figures 5(o) and 5(q) for Mach numbers of 1.11 and 1.12, respectively, were similar to those obtained on the wing at a Mach number of 0.99 at a somewhat lower angle of attack. The level of the negative pressure coefficient on the upper surface was somewhat lower than that for a Mach number of 0.99. The maximum difference between pressure coefficients on the upper and lower surfaces of the wing at the 95-percent-chord location was 100 percent of free-stream dynamic pressure q on the 40-percent-semispan station at a Mach number of 1.11 and an angle of attack of 18° (fig. 5(o)).

Fuselage

The most notable Mach number effect on the fuselage longitudinal pressure distributions at an angle of attack of 0° was the appearance of a region of relatively high negative pressure coefficient near the rearward end of the fuselage and a decrease in negative pressure coefficient over the fuselage nose at supersonic speeds. (Compare figs. 7(a) and 10(r).)

When the angle of attack was increased from 0° to 20°, the value of negative pressure coefficient over the nose upper surface and aft portion of the lower surface of the fuselage increased (figs. 7(a) to 10(t)), with the most negative values of pressure coefficient occurring along the two meridians C and D nearest the side of the fuselage.

At an angle of attack of 12° a local region of relatively high negative pressure coefficients developed at the nose of the upper half of the fuselage (figs. 7(b), 10(a), 10(d), 10(g), 10(j), 10(m), 10(p), and 10(s)). Increasing the angle of attack to 20° increased the level and extent of this region (figs. 8, 10(b), 10(e), 10(h), 10(k), 10(n), 10(q), and 10(t)). It may be noted also that the level of negative pressure coefficients over the rearward end of the upper half of the fuselage remained relatively high throughout the angle-of-attack range investigated and thus departed considerably from the distributions predicted by usual flow theory.

Fuselage with Wing

The addition of the wing to the fuselage had a pronounced effect on the fuselage pressures, especially in the region of the wing blanketed by the fuselage, as shown in figures 6(a), 6(b), 6(c), 8, and 10(a) to 10(s). The wing effect extended somewhat in front of the

leading edge of the wing-fuselage juncture up to a Mach number of 1.02 (figs. 10(l) to 10(n)), and to the rear of this juncture at all Mach numbers investigated. At Mach numbers above 1.11, it was shown in figures 10(o) to 10(t) that the effect of the presence of the wing on the fuselage pressures in front of the wing-fuselage juncture was considerably reduced throughout the angle-of-attack range investigated. A rearward shift in the region of relatively high negative pressure coefficients on the upper half of the fuselage and relatively high positive pressure coefficients on the lower half of the fuselage was exhibited when the Mach number was increased. This rearward shift was greatest on the top and bottom meridians, especially in the Mach number range of 0.97 and beyond for an angle of attack of 0°, and in the Mach number range of 0.89 and above for the angle-of-attack cases.

In the region of the wing-fuselage juncture, the longitudinal distributions of pressure followed closely the general chordwise trends with increase in Mach number and angle of attack indicated by the wing, especially the inboard stations.

The relatively rapid pressure recovery over the most rearward portions of the fuselage may be attributed in part to the interference from the sting that supported the model in the tunnel.

0° angle of attack.- A relatively rapid rearward shift in maximum negative pressure coefficient was noted on the top meridian of the fuselage at an angle of attack of 0° when the Mach number was increased from 0.94 to 0.97 (figs. 10(c) and 10(f)). This peak did not appear to shift farther with increase in Mach number to 1.13; however, the positive pressure coefficient peak was noted to shift forward between Mach numbers of 0.97 and 0.99 (figs. 10(f) and 10(i), respectively), then rearward with continuing Mach number to 1.13. It is also of interest to note that the level of negative pressure coefficients aft of the wing-fuselage juncture began to increase above that of the fuselage alone at a Mach number of 0.97 (fig. 10(f)). At a Mach number of 0.99, these high negative pressure coefficients spread rearward to approximately 85 percent fuselage length (fig. 10(i)). When supersonic Mach numbers of 1.11 and 1.13 were reached, the pressure coefficients following the pressure recovery at the trailing edge of the wing-fuselage juncture were the same on the fuselage with wing as for the fuselage without wing (figs. 10(o) and 10(r)).

4° and 8° angle of attack.- A considerable increase in the level of positive and negative pressure coefficients on the fuselage was noted when the angle of attack was increased from 4° to 8°. As a result, the loads imposed on the fuselage by the wing were greatly intensified. In figure 10, it may be seen that, for Mach numbers of 0.94 and above, the region of relatively high negative pressure coefficients over the

rearward portion of the wing stations nearest the fuselage had a greater influence on the fuselage pressures than the wing leading-edge negative pressure coefficients. The negative pressure coefficient peak on the forward portion of the inboard stations of the wing (fig. 5), appeared to be more or less localized on the wing. The trends for increasing Mach number were the same as noted for an angle of attack of 0°. A rearward shift in the region of relatively high negative pressure coefficient on the upper half of the fuselage with increase in Mach number indicated a small rearward shift in center of loading might occur on the fuselage.

12°, 18°, and 20° angles of attack.- At an angle of attack of 12°, the pressure diagrams are similar to those shown for 8°. At angles of attack of 18° and 20° in the supersonic speed range, a discontinuity in the negative pressure coefficients was exhibited adjacent to the pressure recovery gradient rearward of the wing-fuselage juncture (figs. 10(k), 10(n), 10(q), and 10(t)).

The pressure diagrams for these high angles of attack also made it evident that the relatively high negative-pressure-coefficient region at the leading edge of the wing had a more pronounced effect on the fuselage pressures than at the lower angles of attack. Other variations in the pressure coefficients for increases in Mach number and angle of attack followed the trends established for the lower angles of attack.

CONCLUSIONS

The results of pressure measurements made on a wing in the presence of a fuselage at transonic speeds indicated that:

1. When the angle of attack was increased up to 20° at Mach numbers from 0.60 to 1.13, a region of relatively high negative pressure coefficients at the leading edge of the wing became broader and spread rearward over the outboard then over the inboard sections of the wing. This spread resulted in considerably greater loads at the trailing edge of the wing. The maximum difference between pressure coefficients on the upper and lower surfaces of the wing at the 95-percent-chord location was 100 percent of free-stream dynamic pressure q on the 40-percent semispan station at a Mach number of 1.11 and an angle of attack of 18°.

2. In general, the level of negative pressure coefficient increased as the Mach number was increased to 0.99, then decreased with further increase in speed up to the highest Mach number tested, 1.13. At the same time the general level of pressure coefficients on the lower surface of the wing became more positive throughout the Mach number range tested.

3. Two pronounced discontinuities in chordwise negative pressure coefficient were evident on the upper surface of the wing in the vicinity of a Mach number of 1.00. One of these discontinuities appeared to originate at the leading edge and the other at the trailing edge of the wing-fuselage juncture. Both extended in a spanwise direction and merged in the region of the wing tip.

The results of pressure measurements made on a fuselage with and without a wing indicated that:

1. At zero angle of attack the negative pressure coefficients over the nose of the fuselage upper surface decreased and a region of relatively high negative pressure coefficients became apparent on the rear portion of the fuselage upper surface as the Mach number was increased to supersonic values.

2. The level of negative pressure coefficients over the rear portion of the fuselage upper surface did not decrease with increase in angle of attack but remained relatively high throughout the angle-of-attack range investigated.

3. Adding the wing to the fuselage greatly increased the level of the pressures in the region of the wing-fuselage juncture, thereby amplifying the load on the fuselage considerably.

4. Increases in Mach number resulted in rearward shifts in regions of relatively high negative pressure coefficient on the fuselage.

Langley Aeronautical Laboratory
National Advisory Committee for Aeronautics
Langley Field, Va.

REFERENCES

1. Loving, Donald L., and Estabrooks, Bruce B.: Transonic-Wing Investigation in the Langley 8-Foot High-Speed Tunnel at High Subsonic Mach Numbers and at a Mach Number of 1.2. Analysis of Pressure Distribution of Wing-Fuselage Configuration Having a Wing of 45° Sweepback, Aspect Ratio 4, Taper Ratio of 0.6, and NACA 65A006 Airfoil Section. NACA RM L51F07, 1951.

2. Osborne, Robert S.: A Transonic-Wing Investigation in the Langley 8-Foot High-Speed Tunnel at High Subsonic Mach Numbers and at a Mach Number of 1.2. Wing-Fuselage Configuration Having a Wing of 45° Sweepback, Aspect Ratio 4.0, Taper Ratio 0.6, and NACA 65A006 Airfoil Section. NACA RM L50H08, 1950.

3. Wright, Ray H., and Ward, Vernon G.: NACA Transonic Wind-Tunnel Test Sections. NACA RM L8J06, 1948.

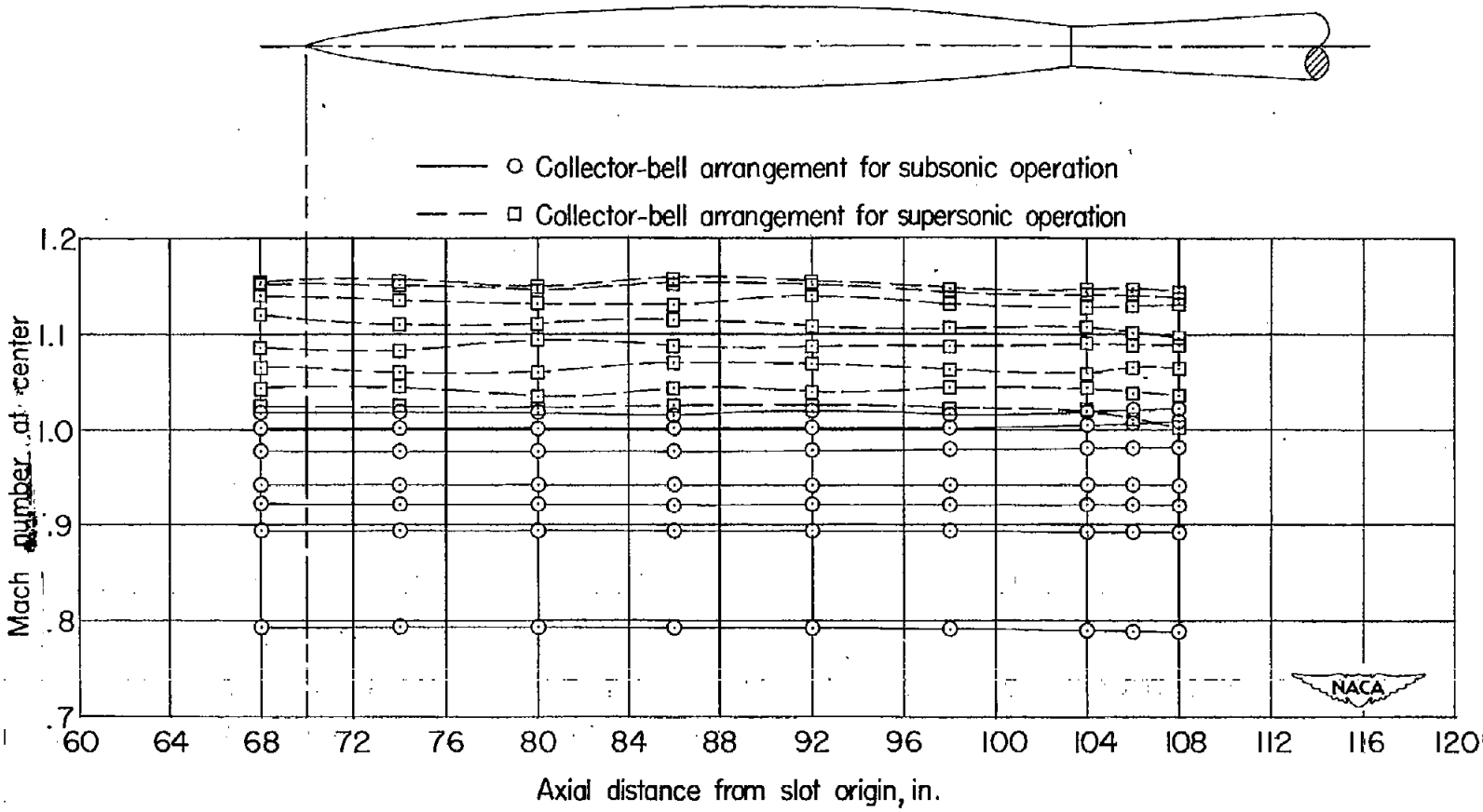

Figure 1.- Mach number distribution in region occupied by the model in the slotted throat of the Langley 8-foot high-speed tunnel.

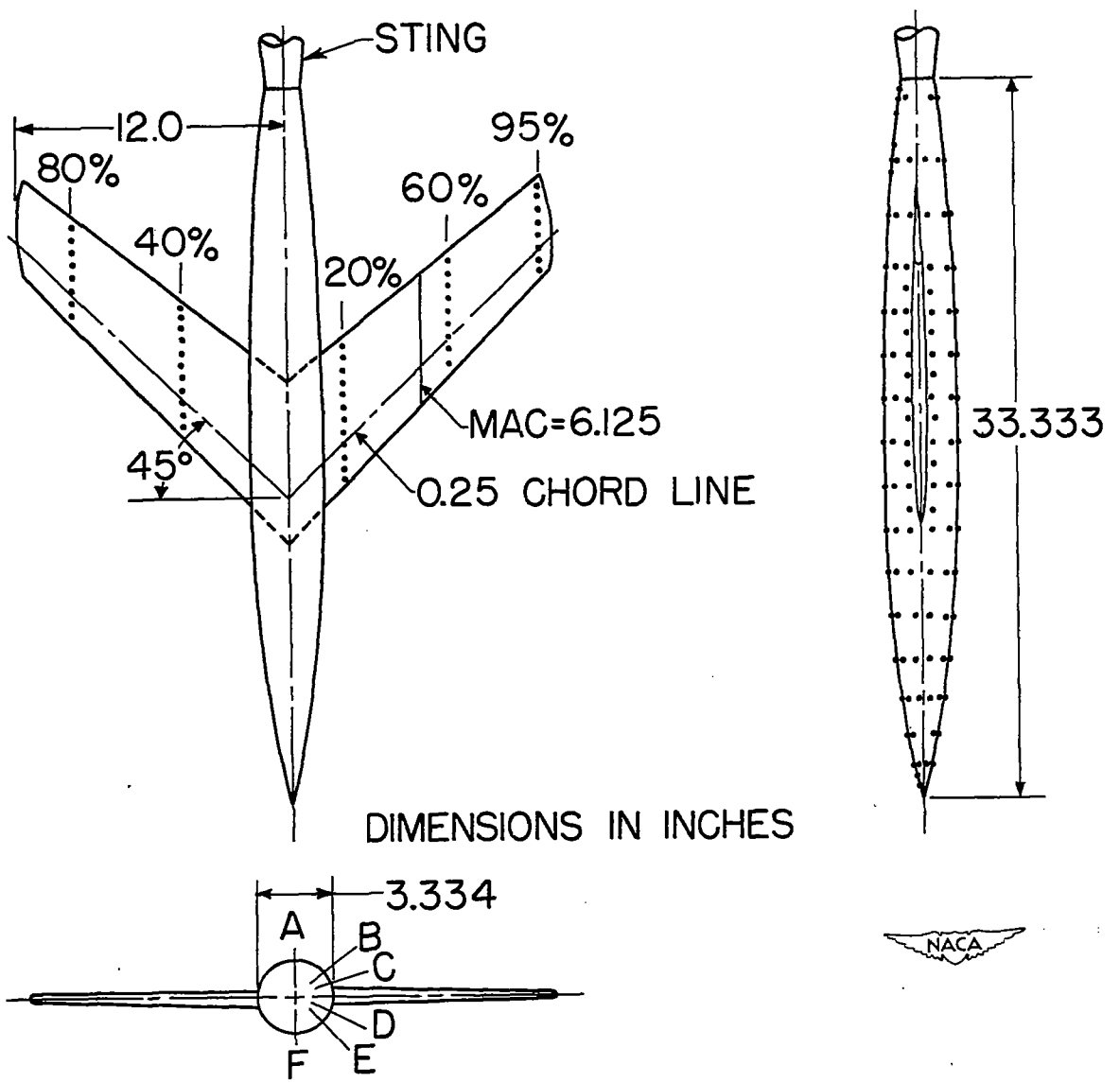

Figure 2.- Details of the wing-fuselage combination investigated in the slotted test section of the Langley 8-foot high-speed tunnel.

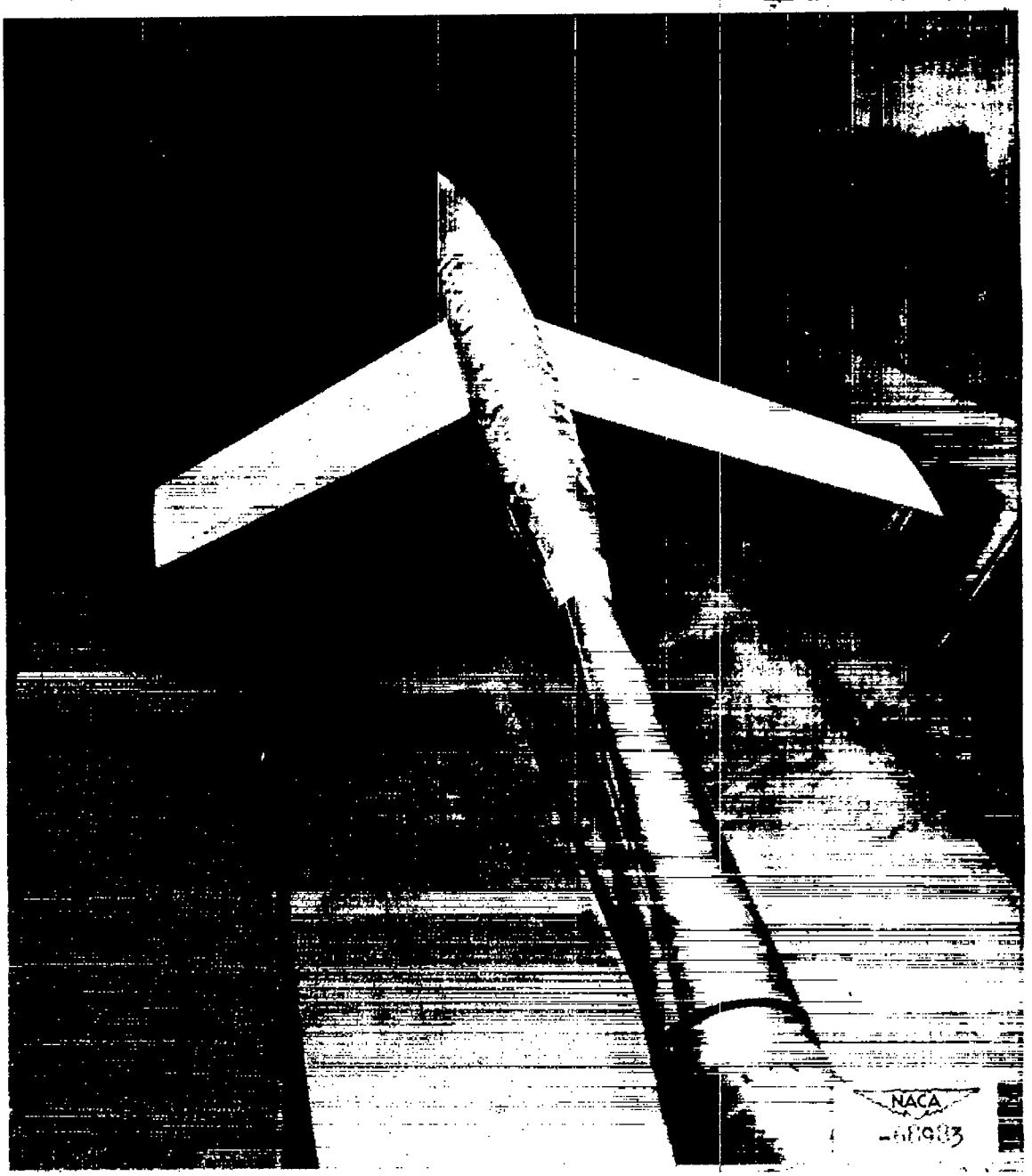

Figure 3.- Photograph of model installed in the slotted test section of the Langley 8-foot high-speed tunnel.

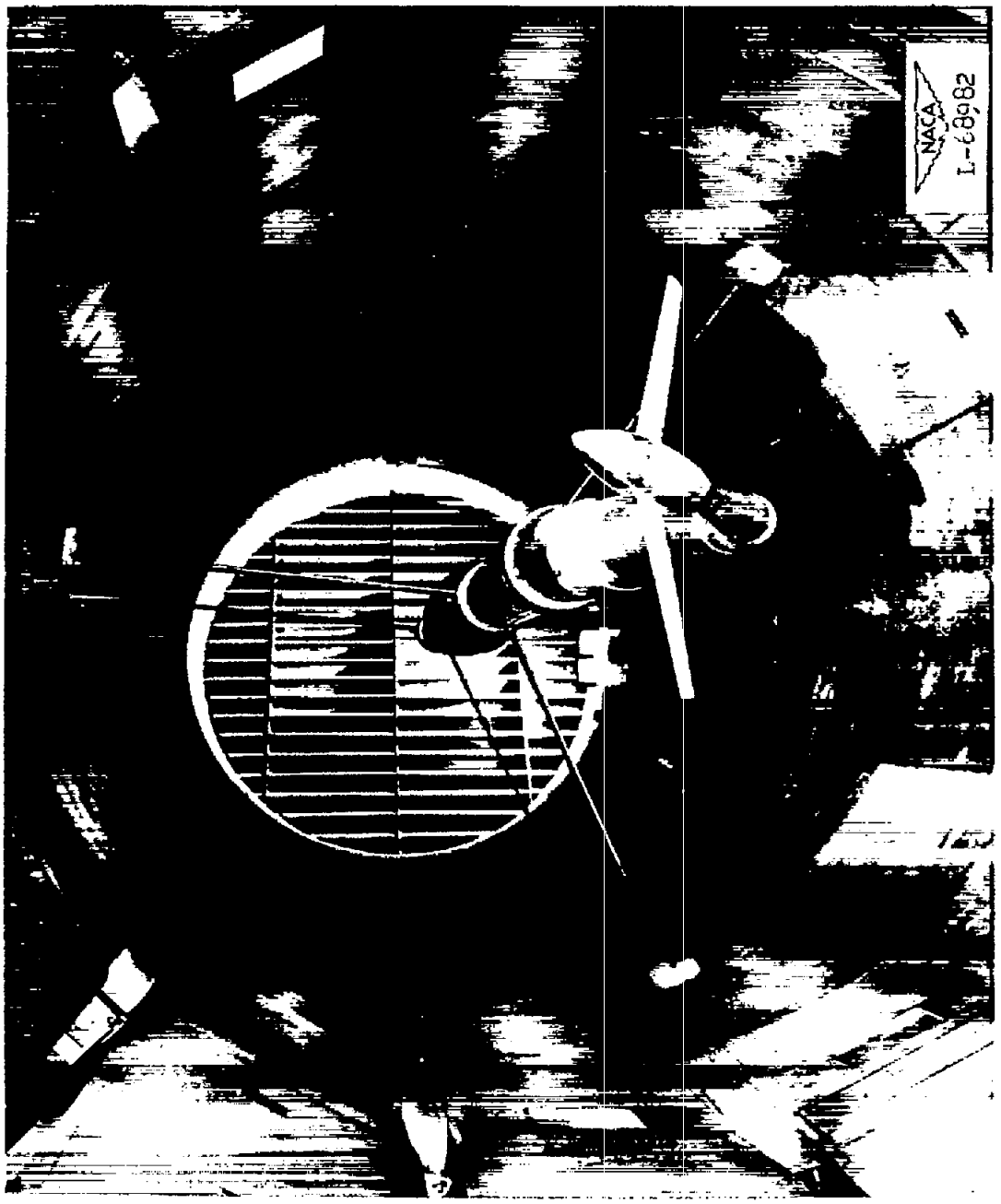

Figure 4.- Photograph of model support system for high angles of attack.

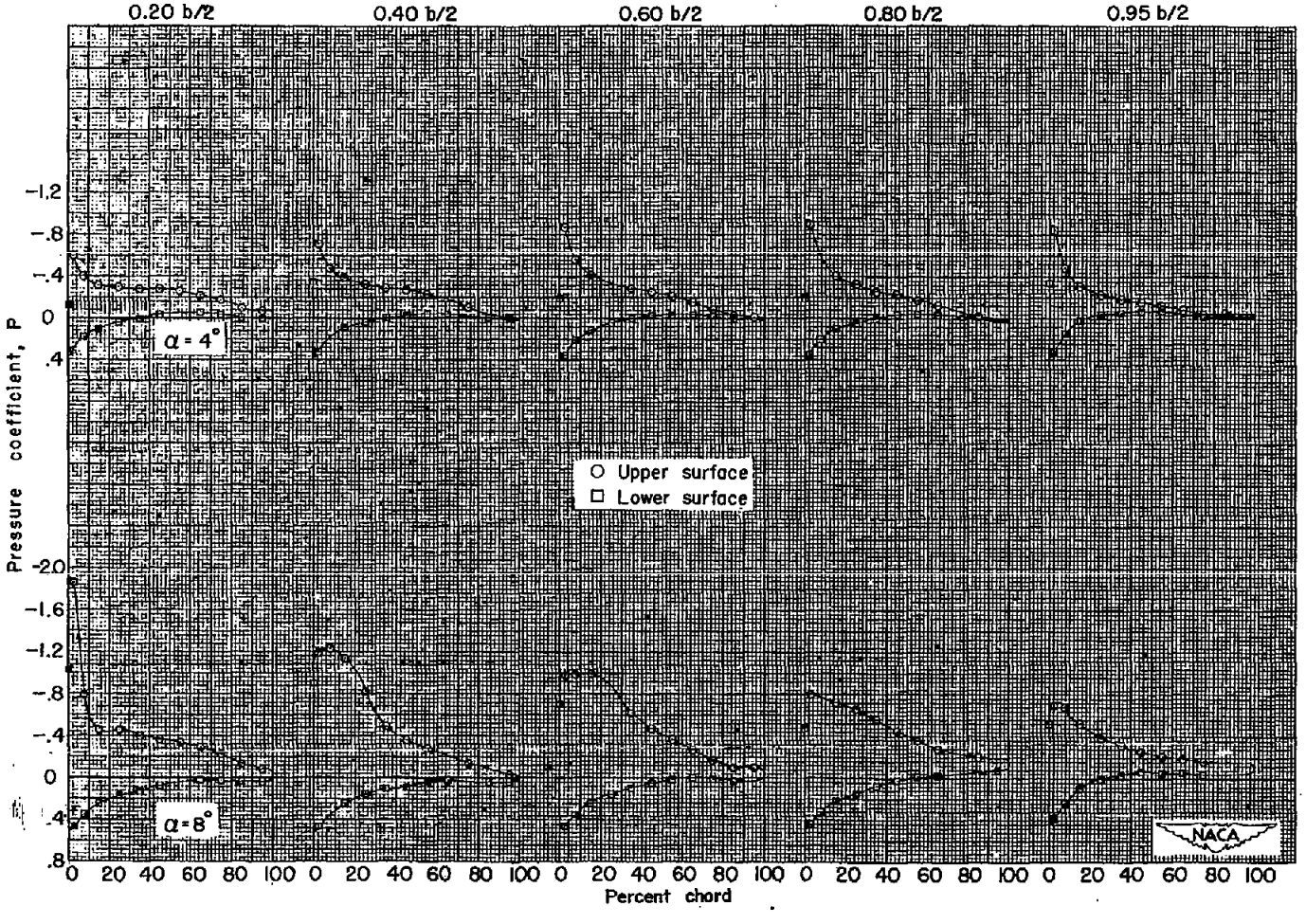

(a) M = 0.60; α = 4° and 8°.

Figure 5.- The chordwise pressure distribution at five spanwise stations on the wing for various angles of attack.

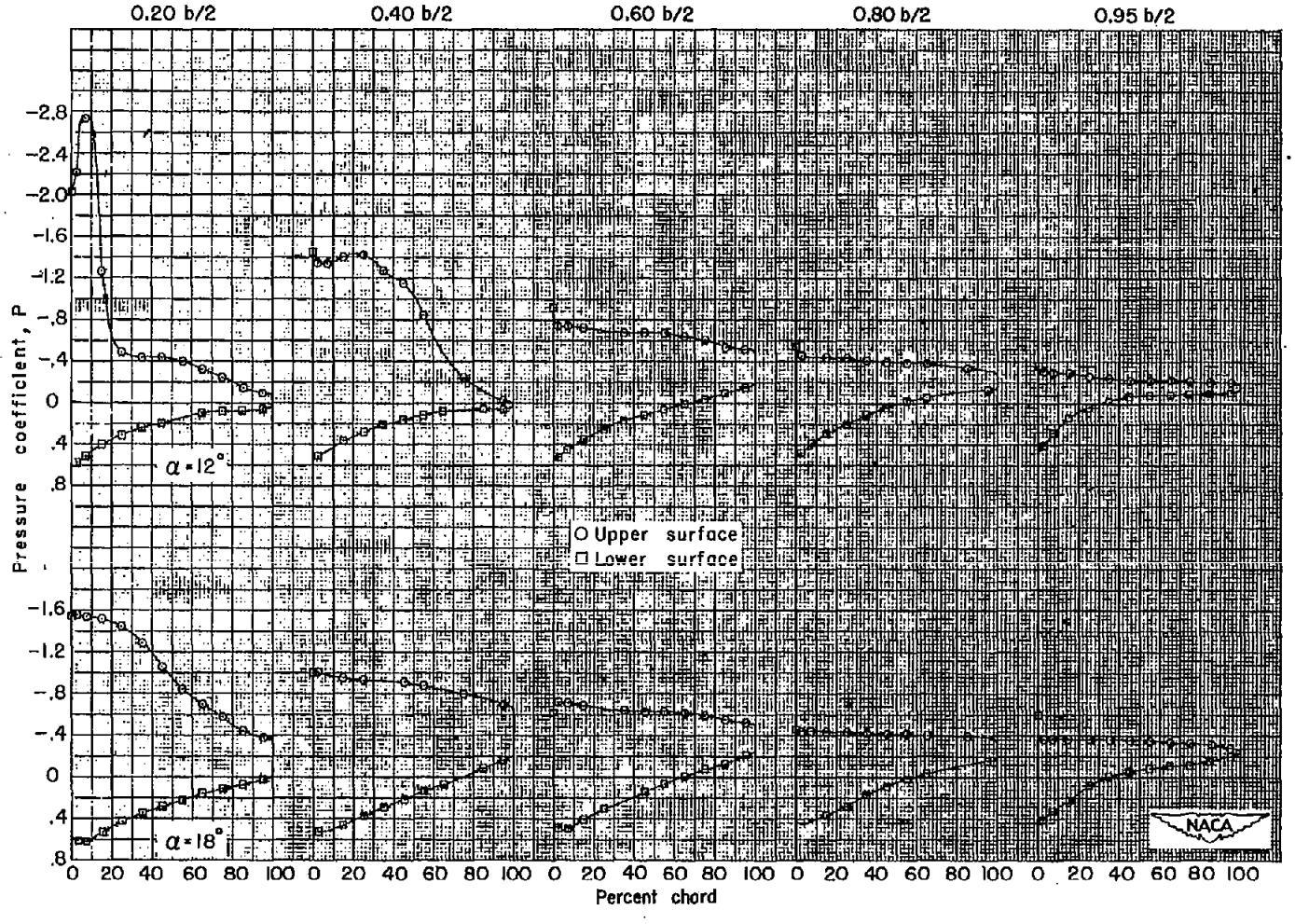

(b) M = 0.60; α = 12° and 18°.

Figure 5.- Continued.

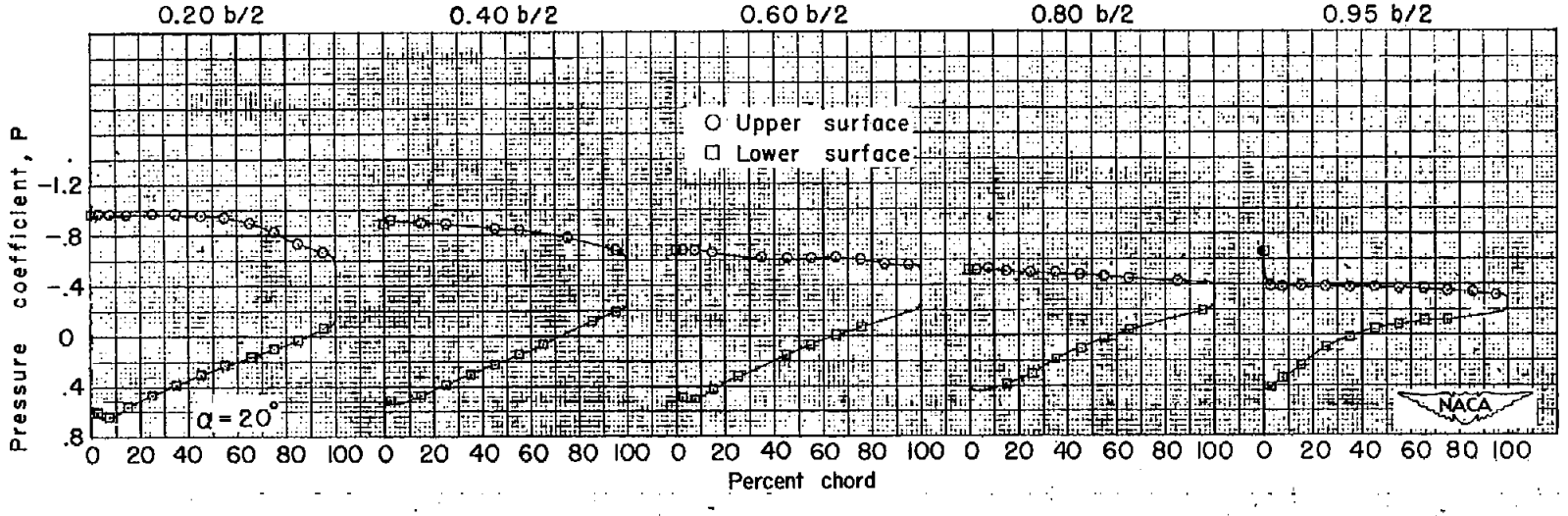

(c) $M = 0.60$; $\alpha = 20^\circ$.

Figure 5.- Continued.

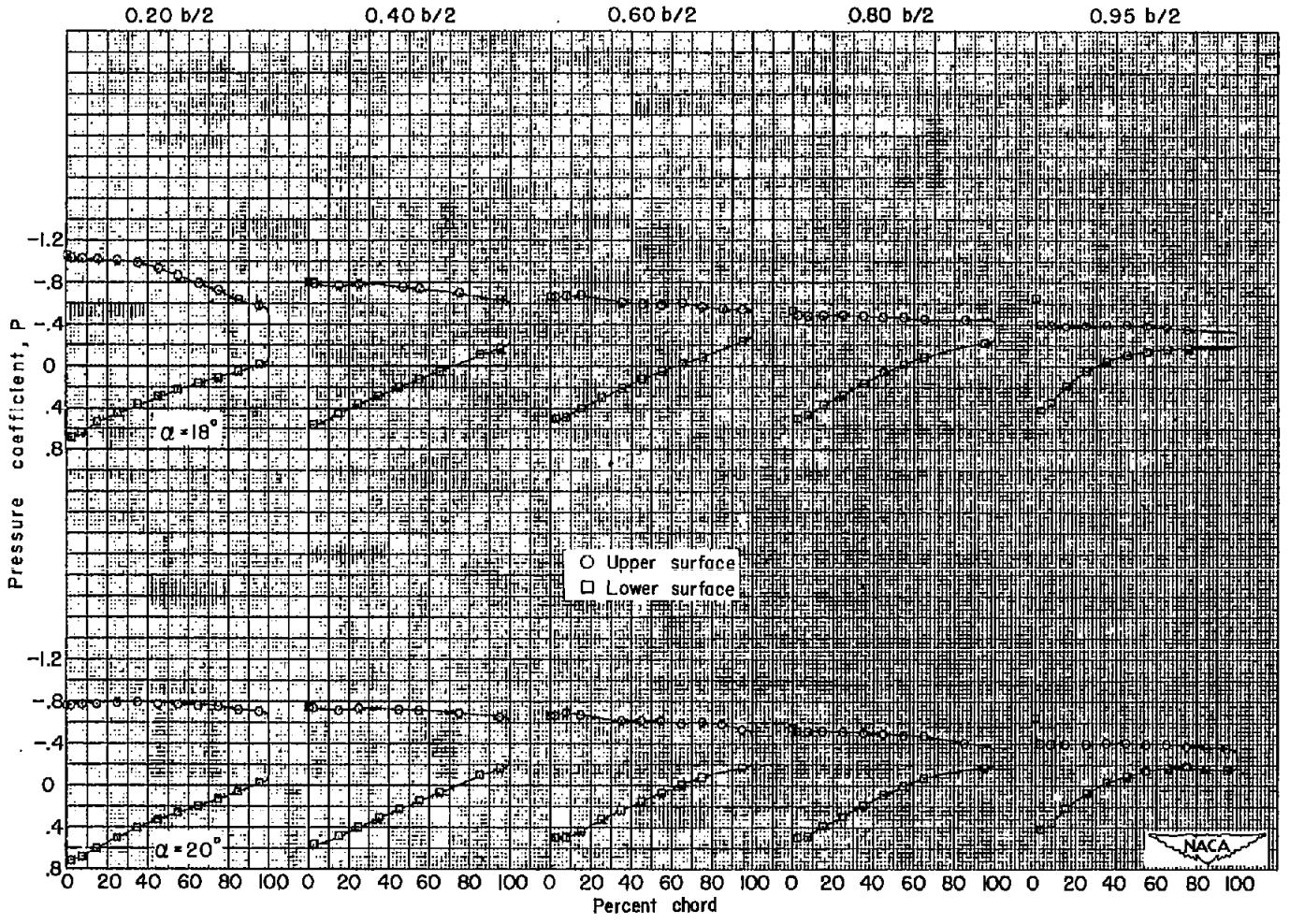

(d) M = 0.79; α = 18° and 20°.

Figure 5.- Continued.

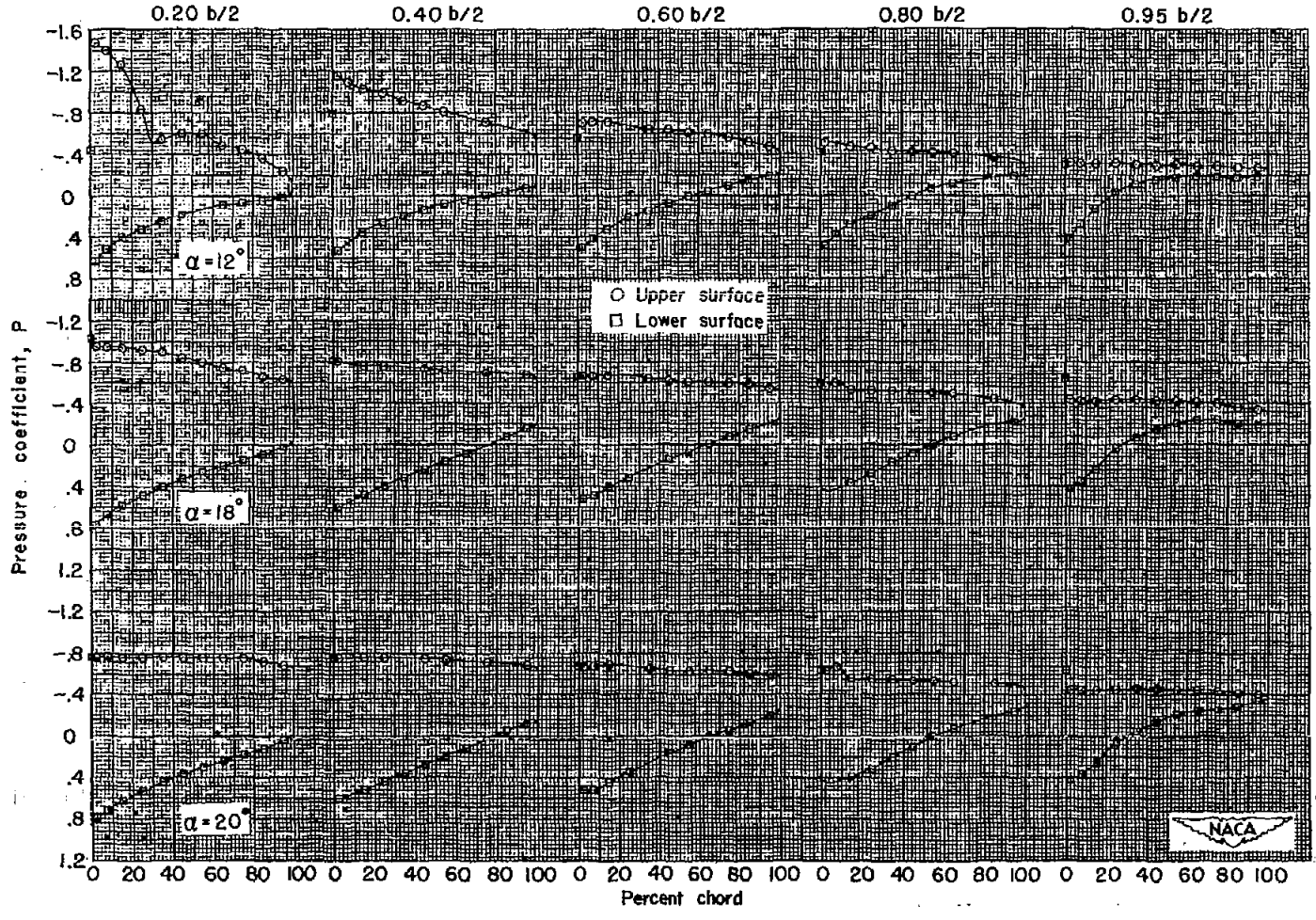

(e) M = 0.89; α = 12°, 18°, and 20°.

Figure 5.- Continued.

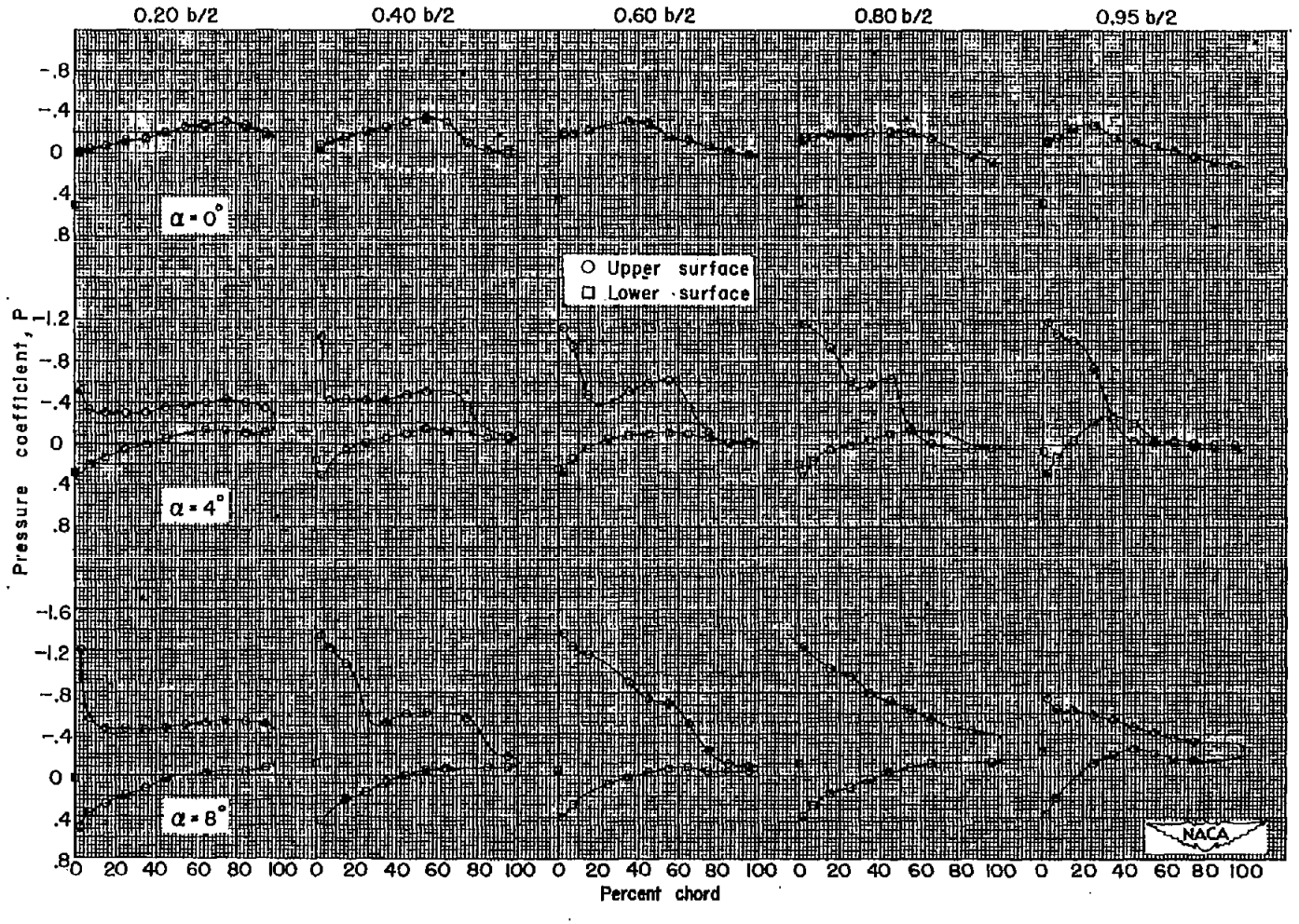

(f) M = 0.94; α = 0°, 4°, and 8°.

Figure 5.- Continued.

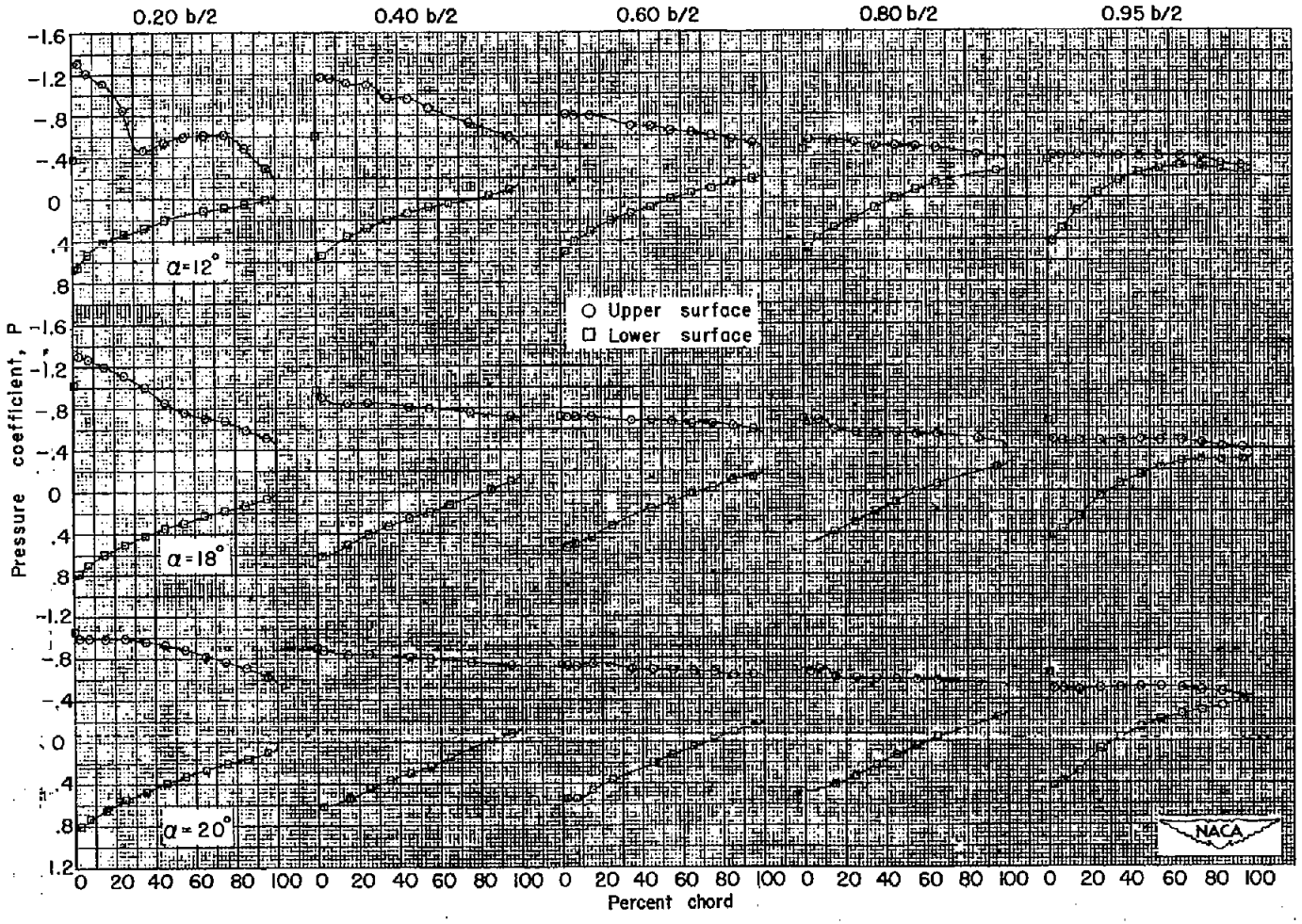

(g) M = 0.94; $\alpha = 12^{\circ}$, 18°, and 20°.

Figure 5.- Continued.

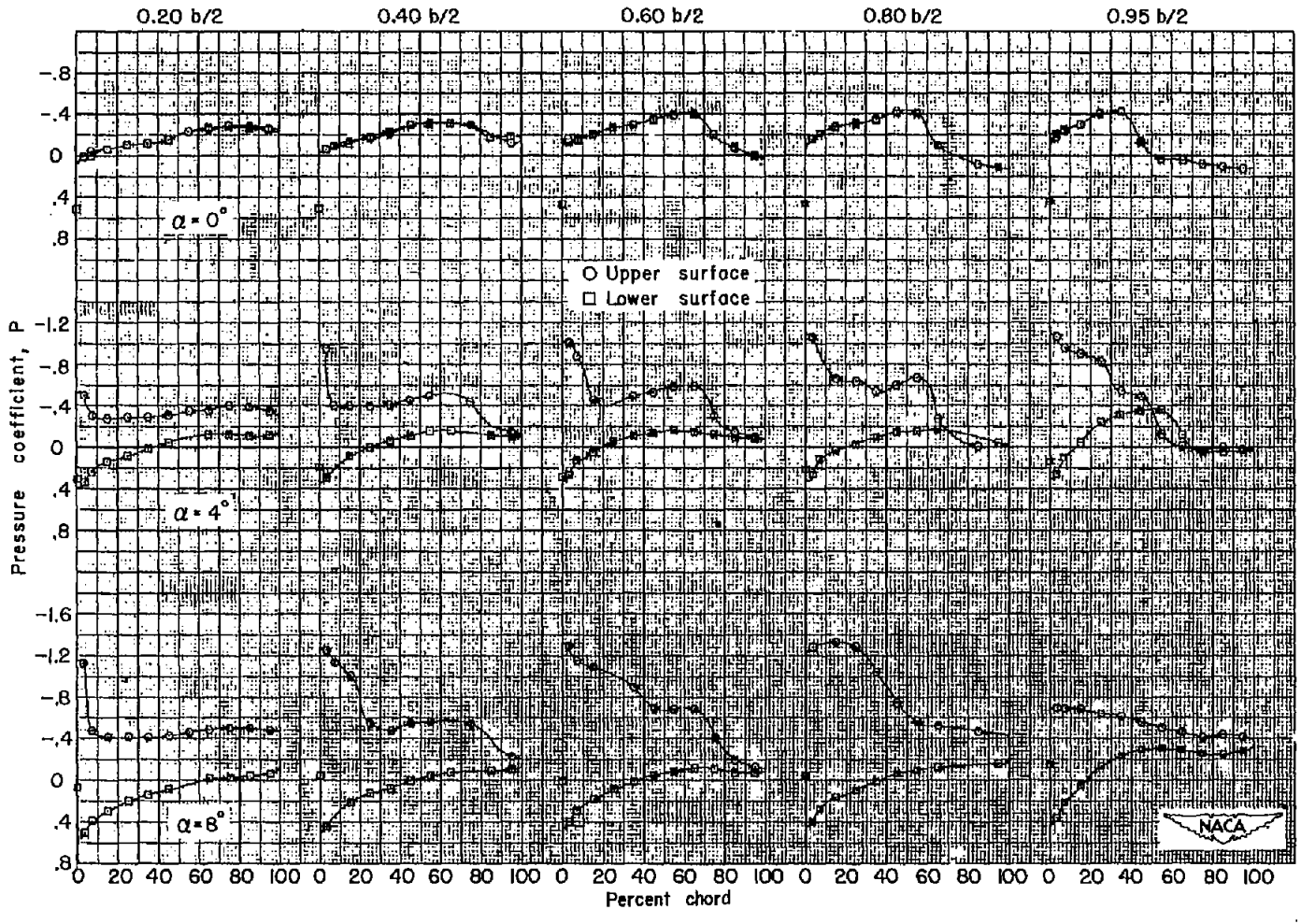

(h) M = 0.97; $\alpha = 0^\circ$, 4°, and 8°.

Figure 5.- Continued.

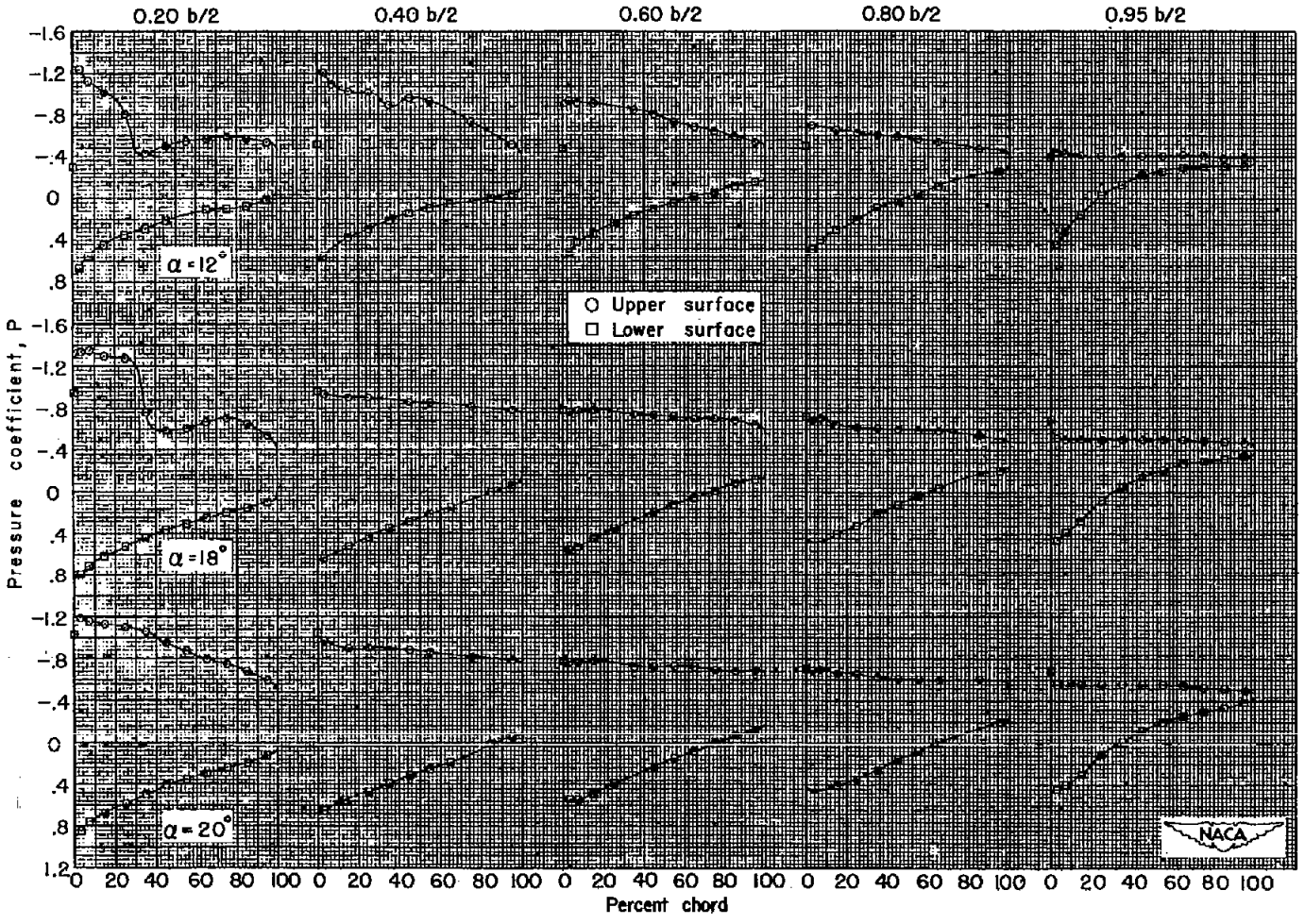

(i) M = 0.97; α = 12°, 18°, and 20°.

Figure 5.- Continued.

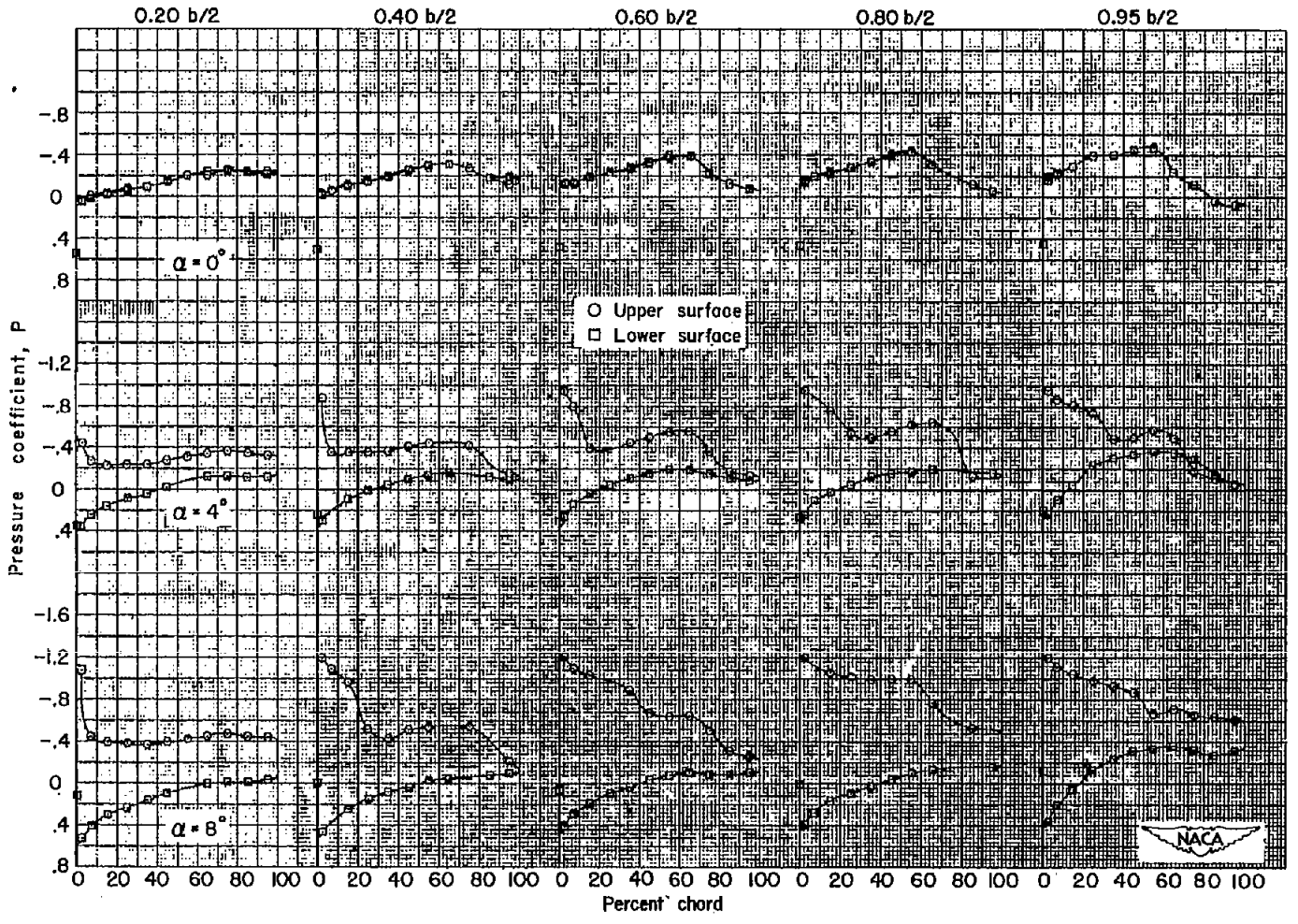

(j) M = 0.99; α = 0°, 4°, and 8°.

Figure 5.- Continued.

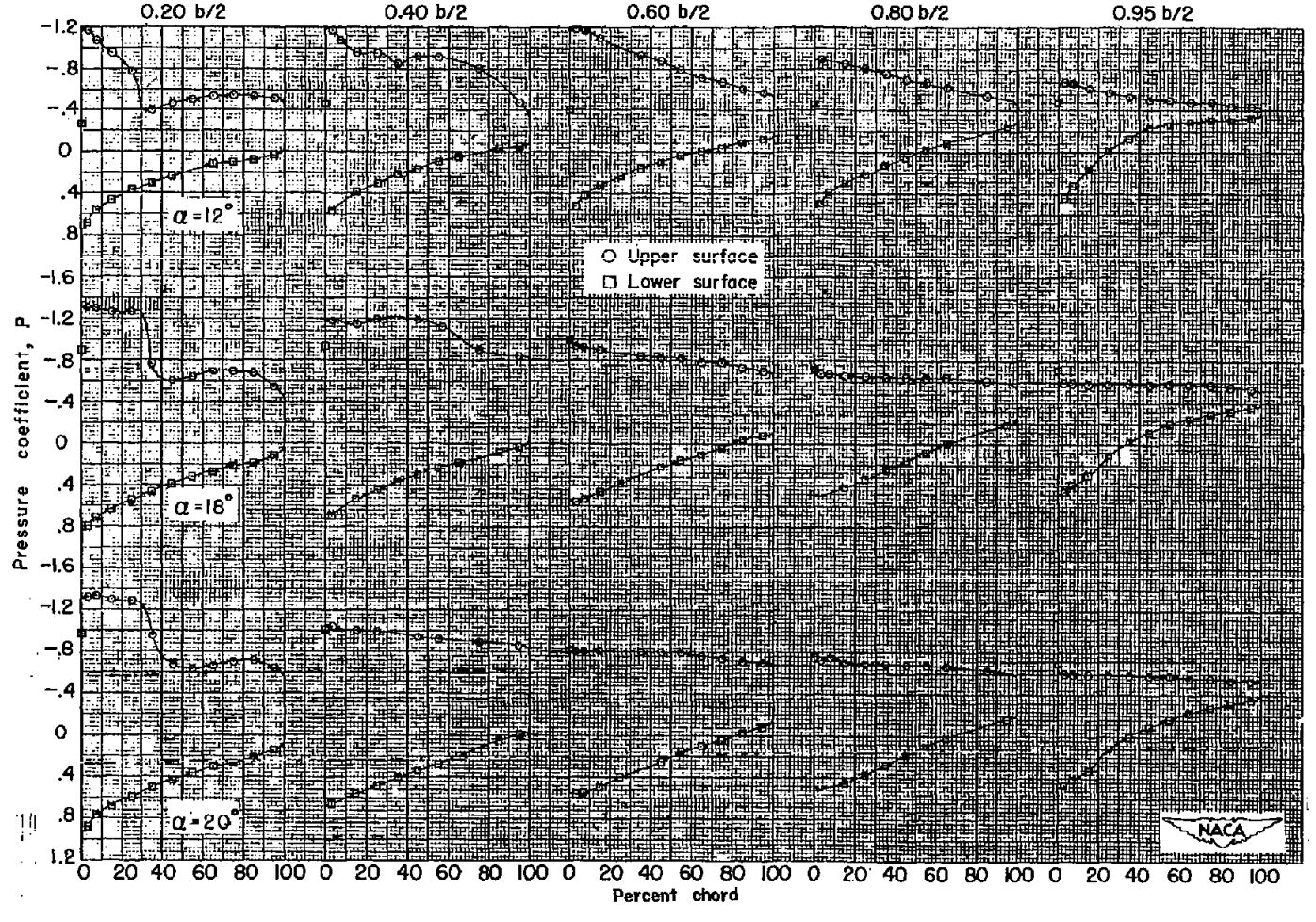

(k) M = 0.99; α = 12°, 18°, and 20°.

Figure 5.- Continued.

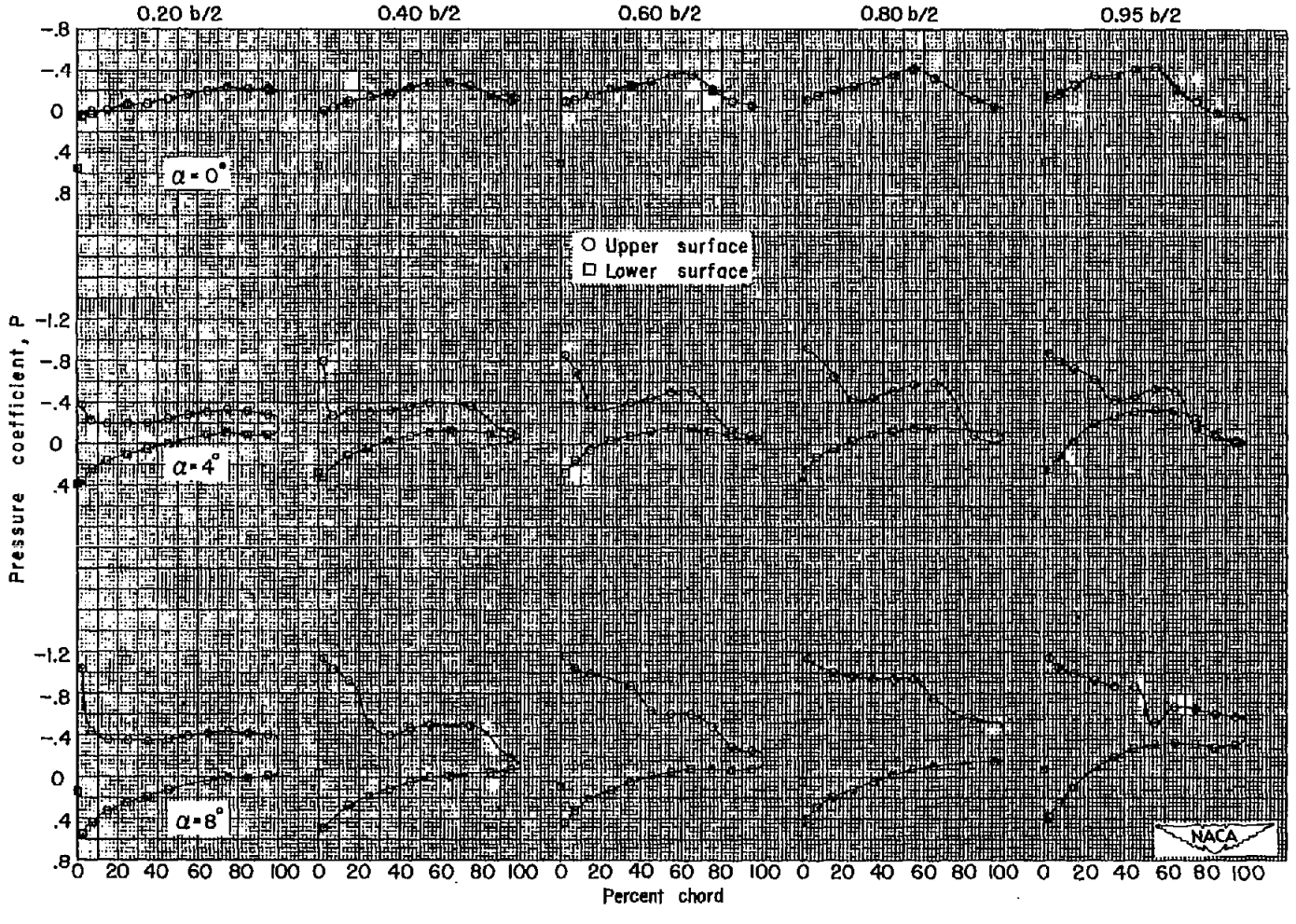

(l) M = 1.02; α = 0°, 4°, and 8°.

Figure 5.- Continued.

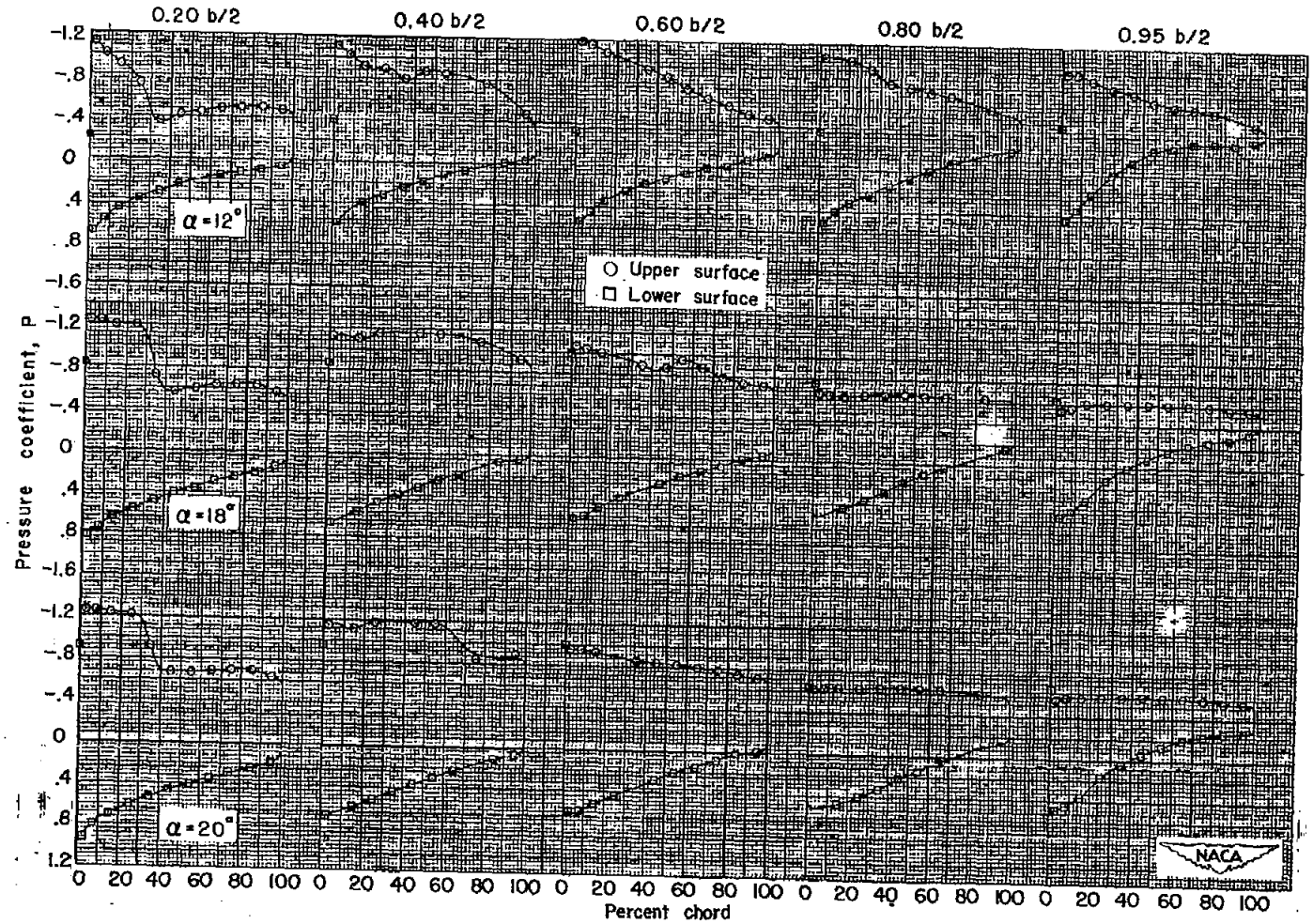

(m) M = 1.02; $\alpha = 12^{\circ}$, 18°, and 20°.

Figure 5.- Continued.

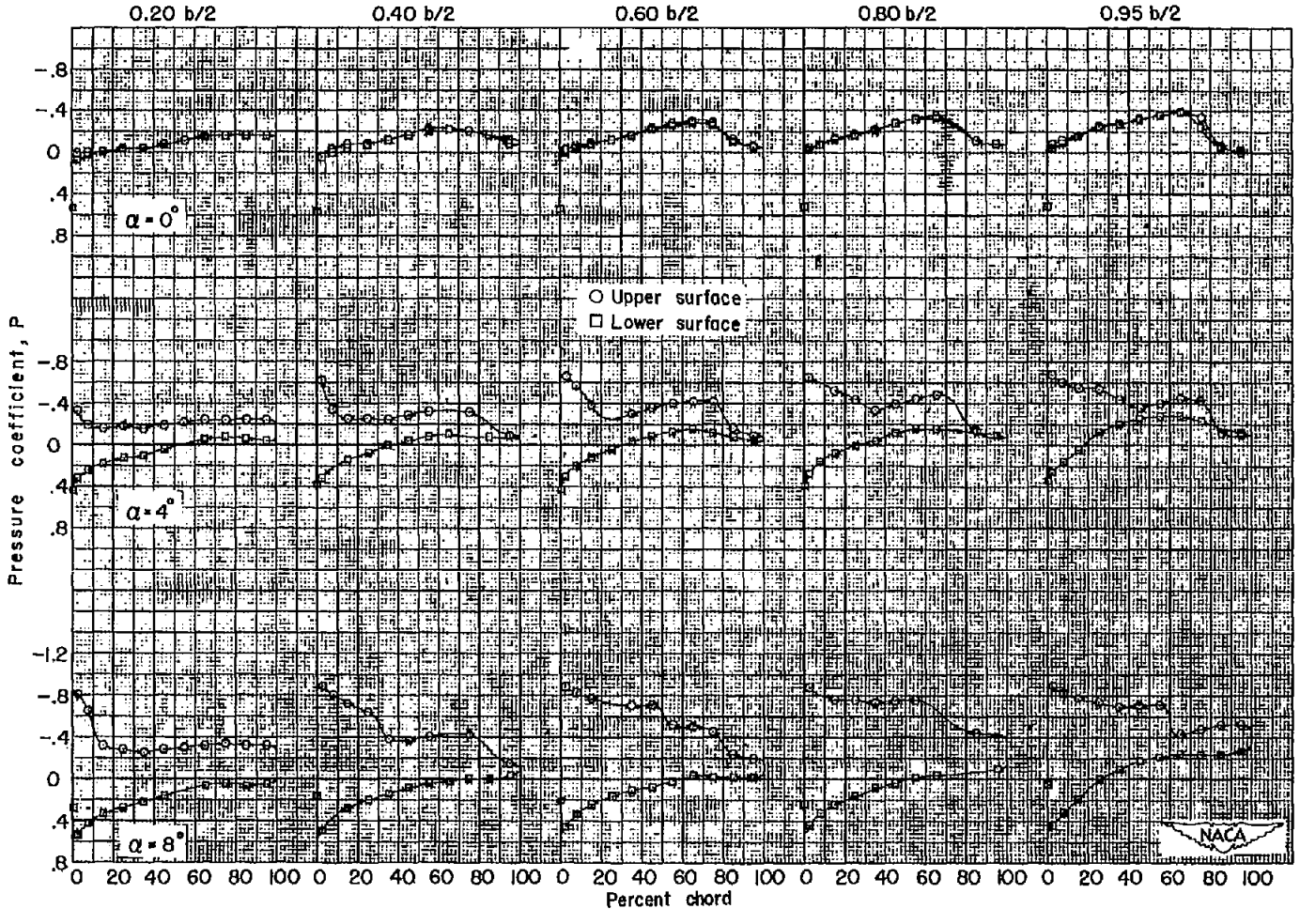

(n) M = 1.11; α = 0°, 4°, and 8°.

Figure 5.- Continued.

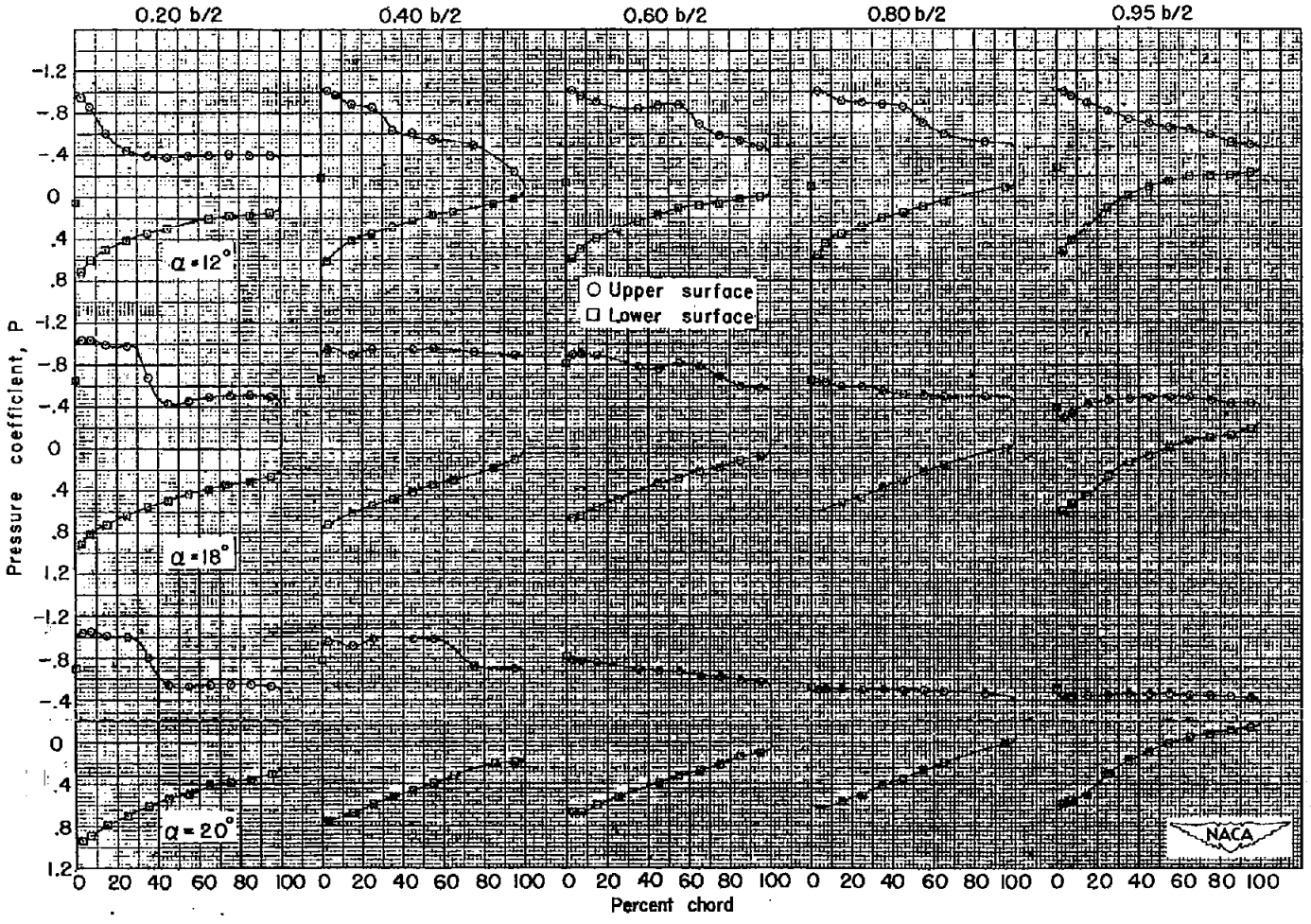

(o) M = 1.11; $\alpha = 12^{\circ}$, 18°, and 20°.

Figure 5.- Continued.

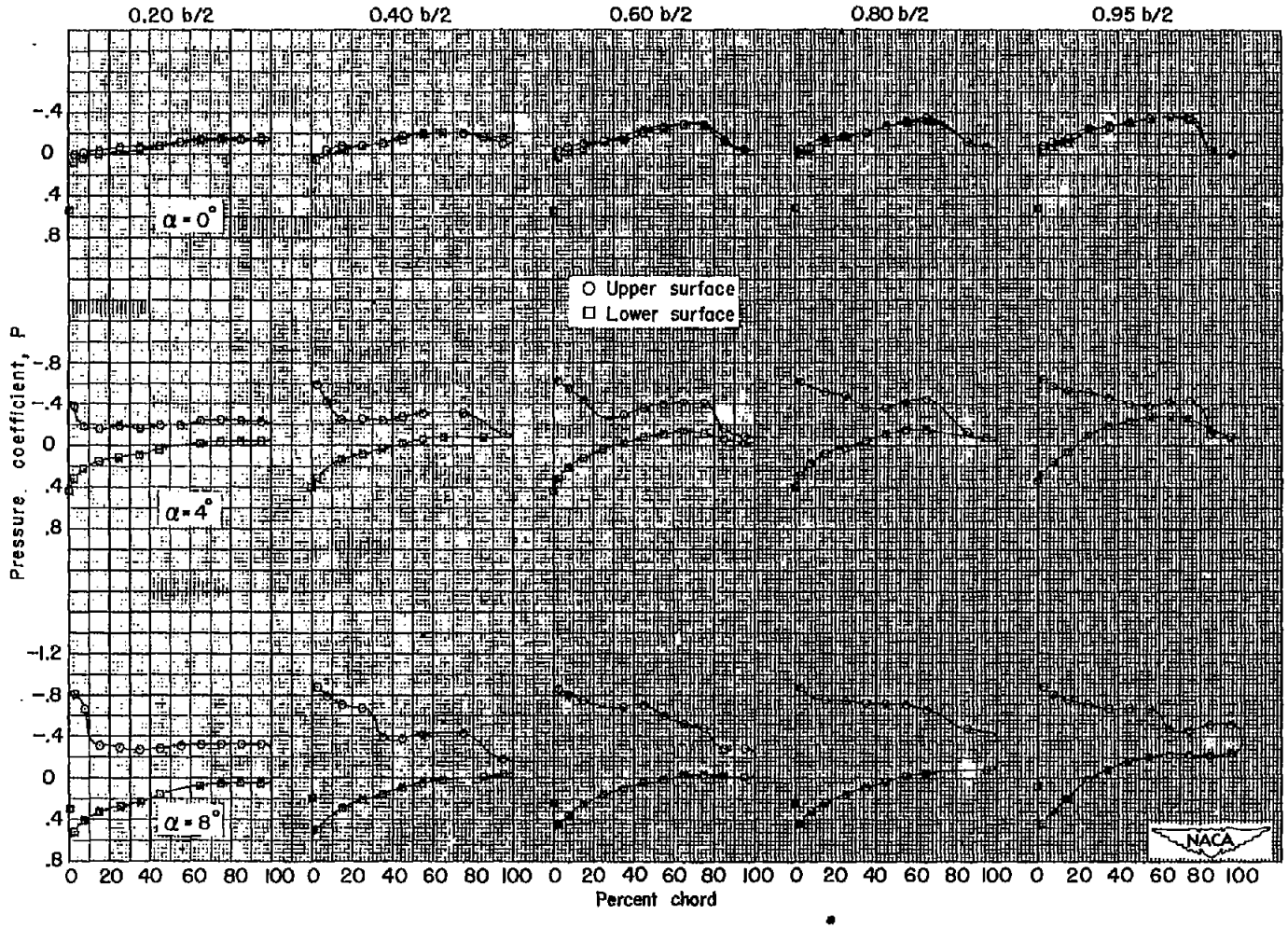

(p) M = 1.13; $\alpha = 0^\circ$, 4°, and 8°.

Figure 5.- Continued.

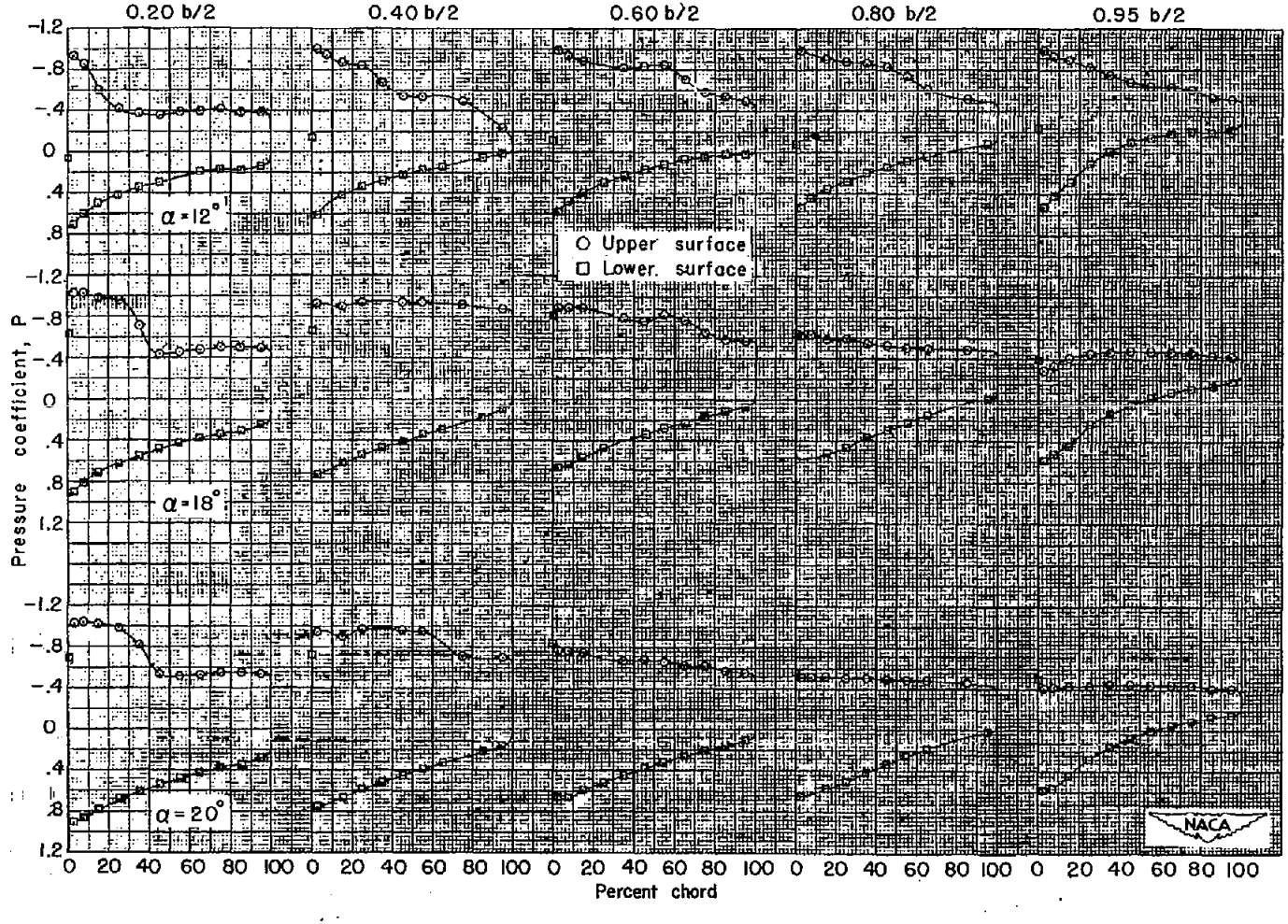

(q) M = 1.12; α = 12°, 18°, and 20°.

Figure 5.- Concluded.

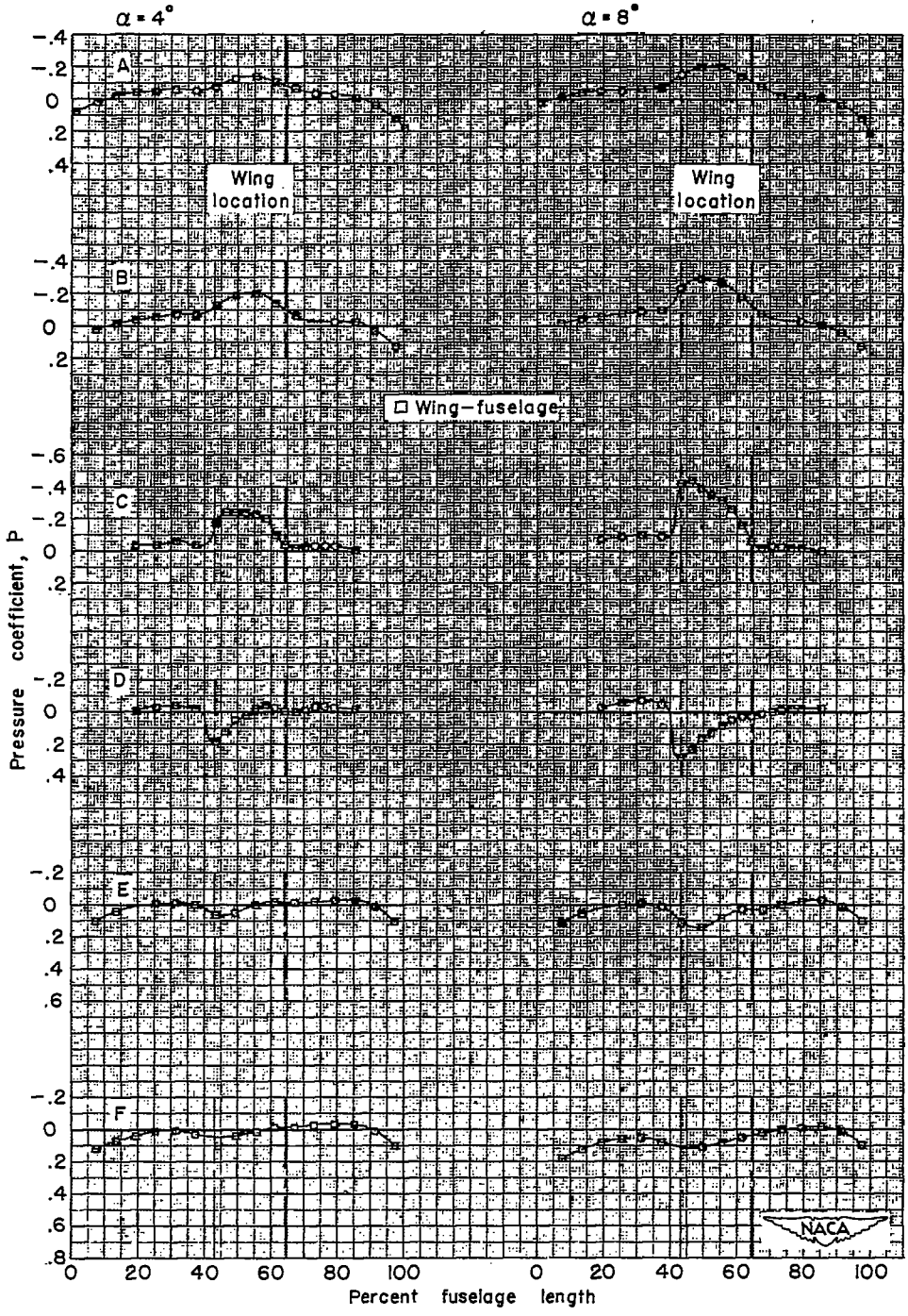

(a) M = 0.60; α = 4° and 8°.

Figure 6.- The longitudinal pressure distribution at six radial locations for the wing-fuselage configuration at various angles of attack.

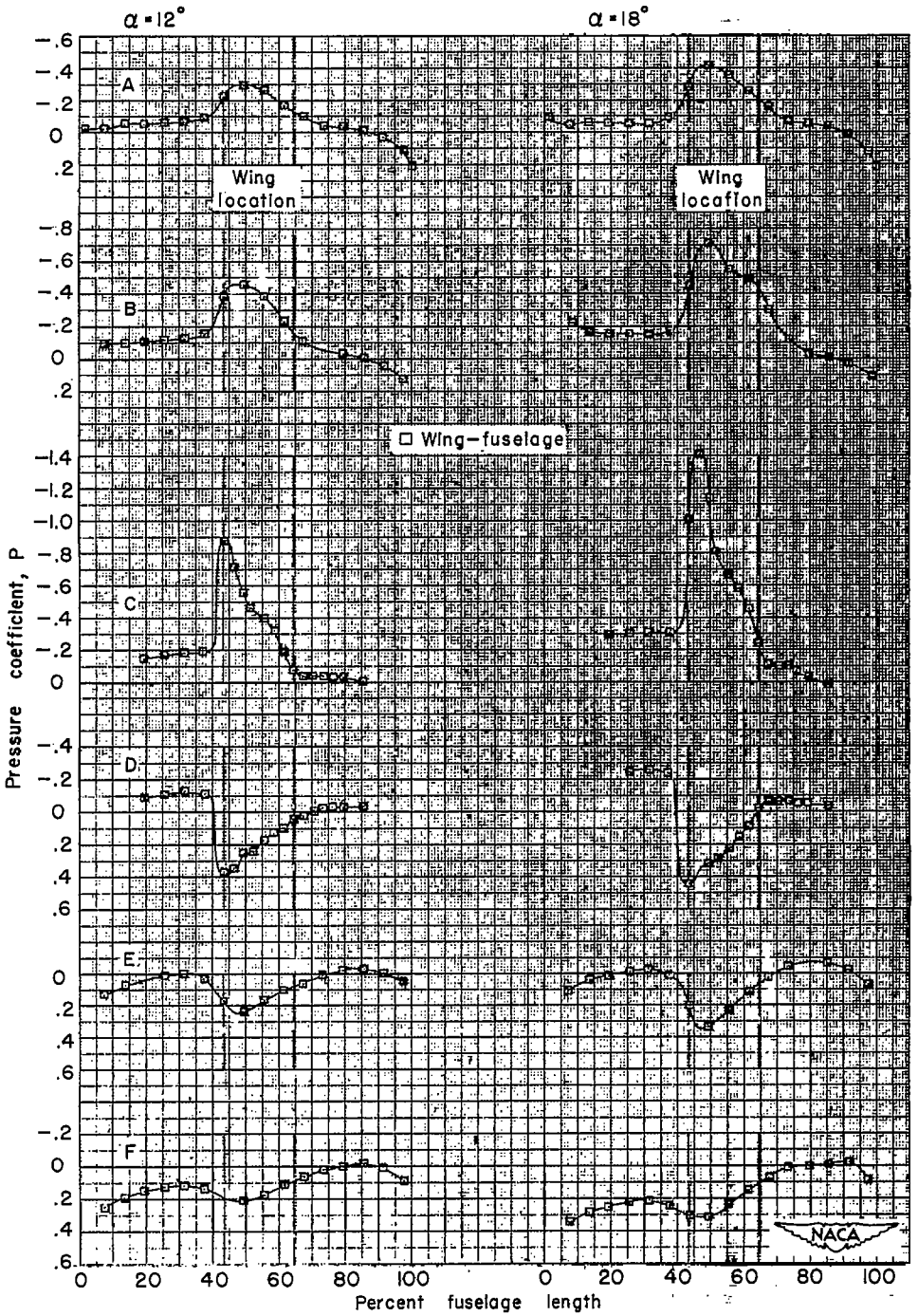

(b) M = 0.60; α = 12° and 18°.

Figure 6.- Continued.

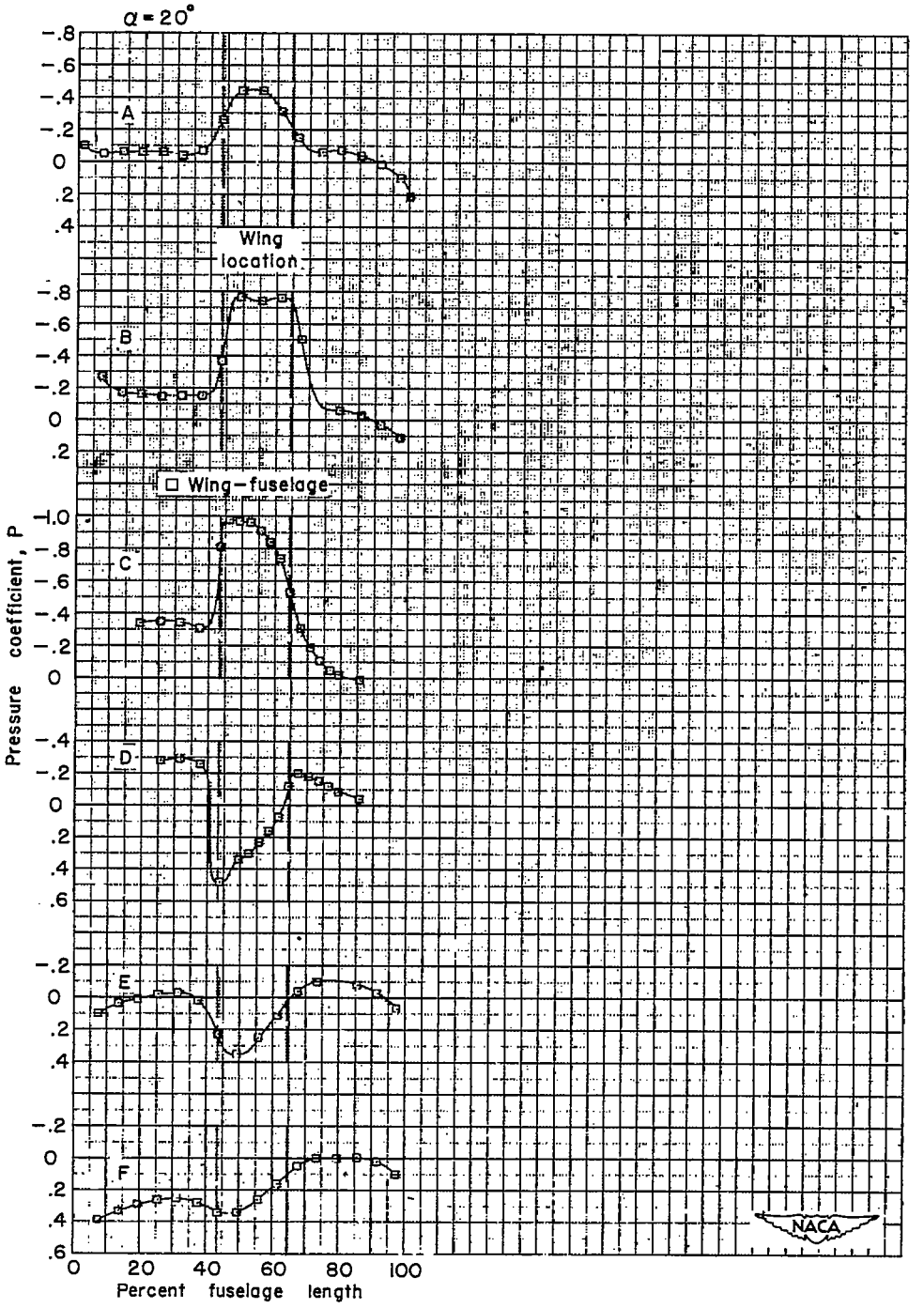

(c) M = 0.60; $\alpha = 20^{\circ}$.

Figure 6.- Concluded.

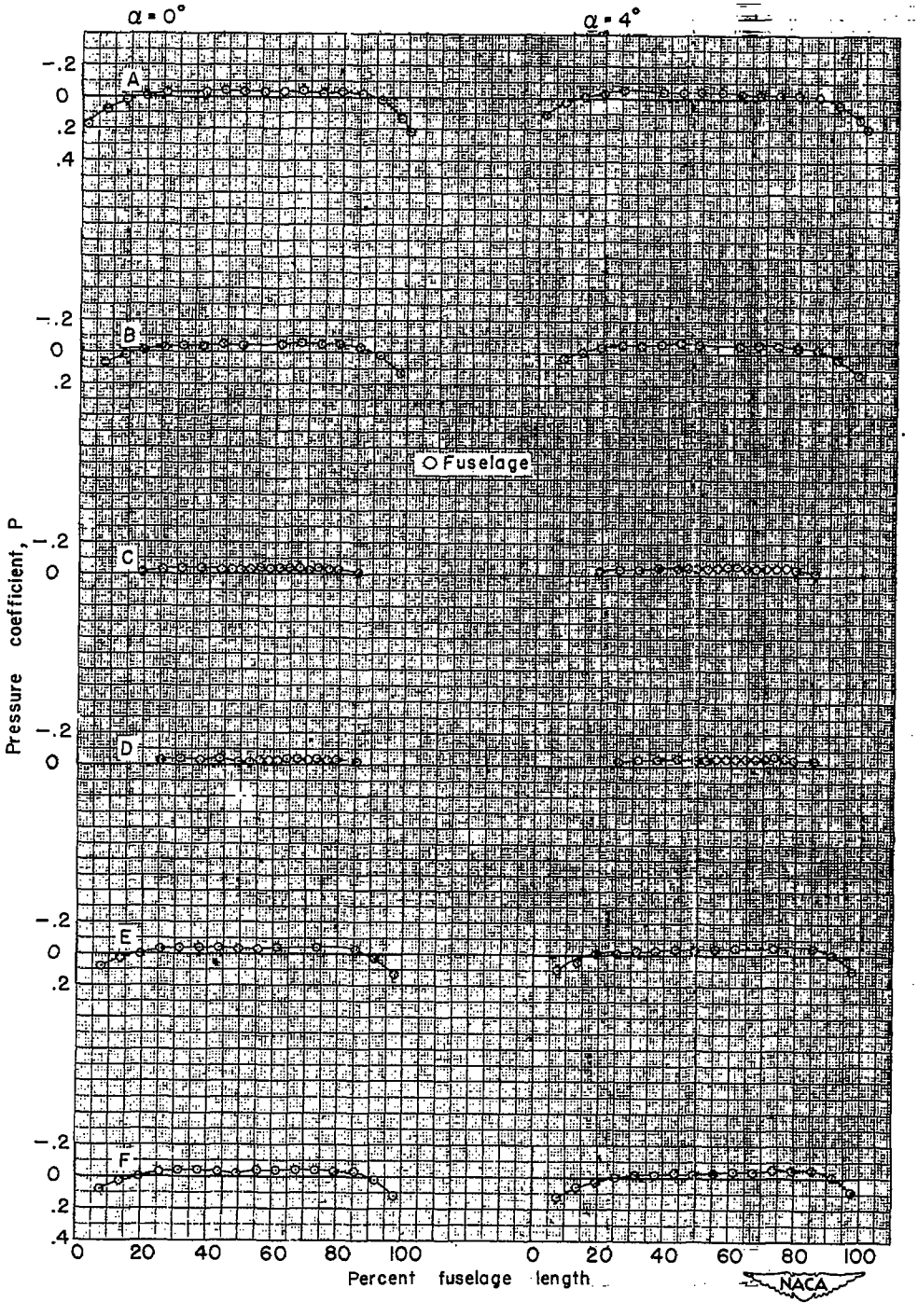

(a) M = 0.79; $\alpha = 0^{\circ}$ and 4°.

Figure 7.- The longitudinal pressure distribution at six radial locations for the fuselage configuration at various angles of attack.

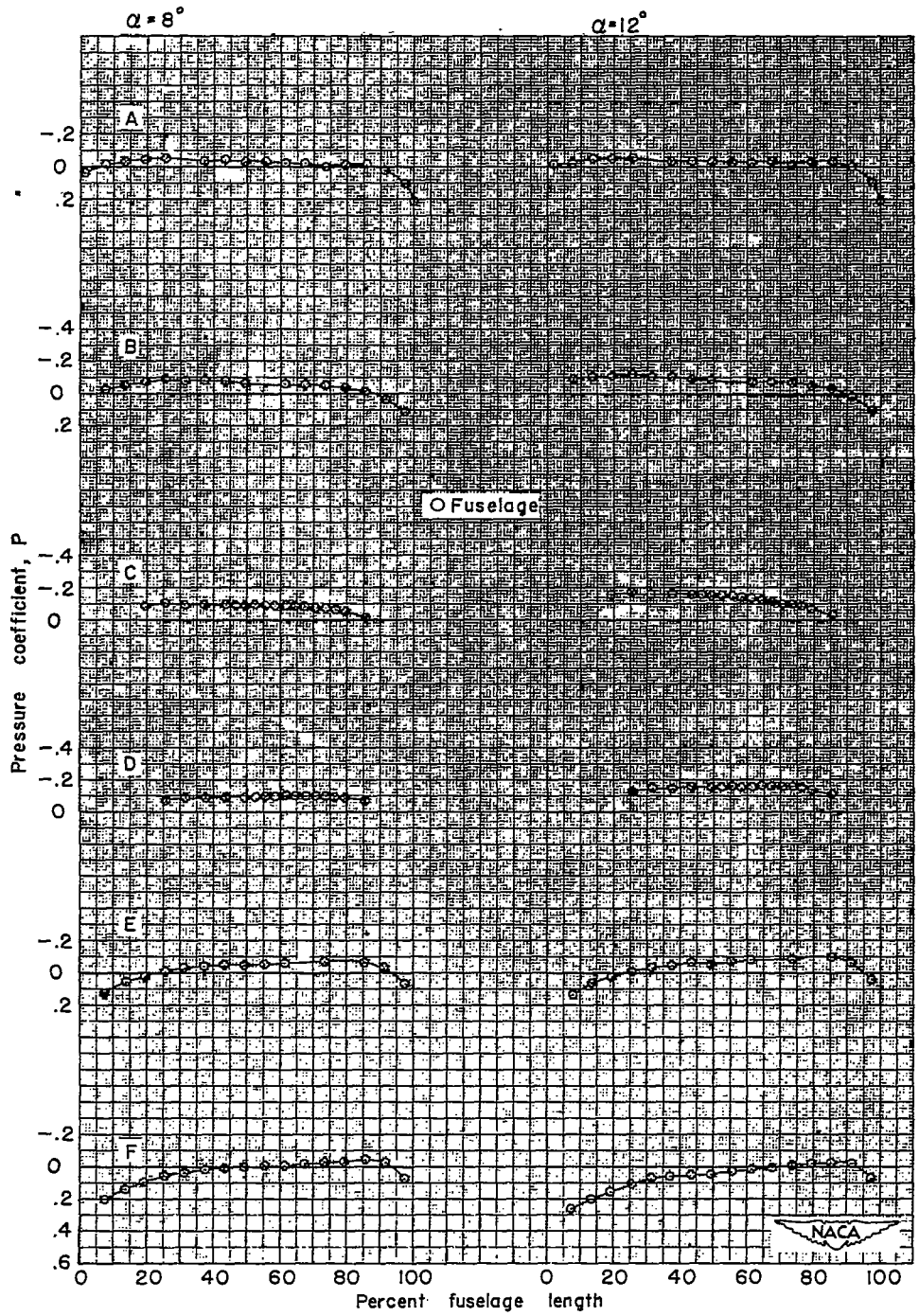

(b) M = 0.79; $\alpha = 8^{\circ}$ and 12°.

Figure 7.- Concluded.

[redacted]

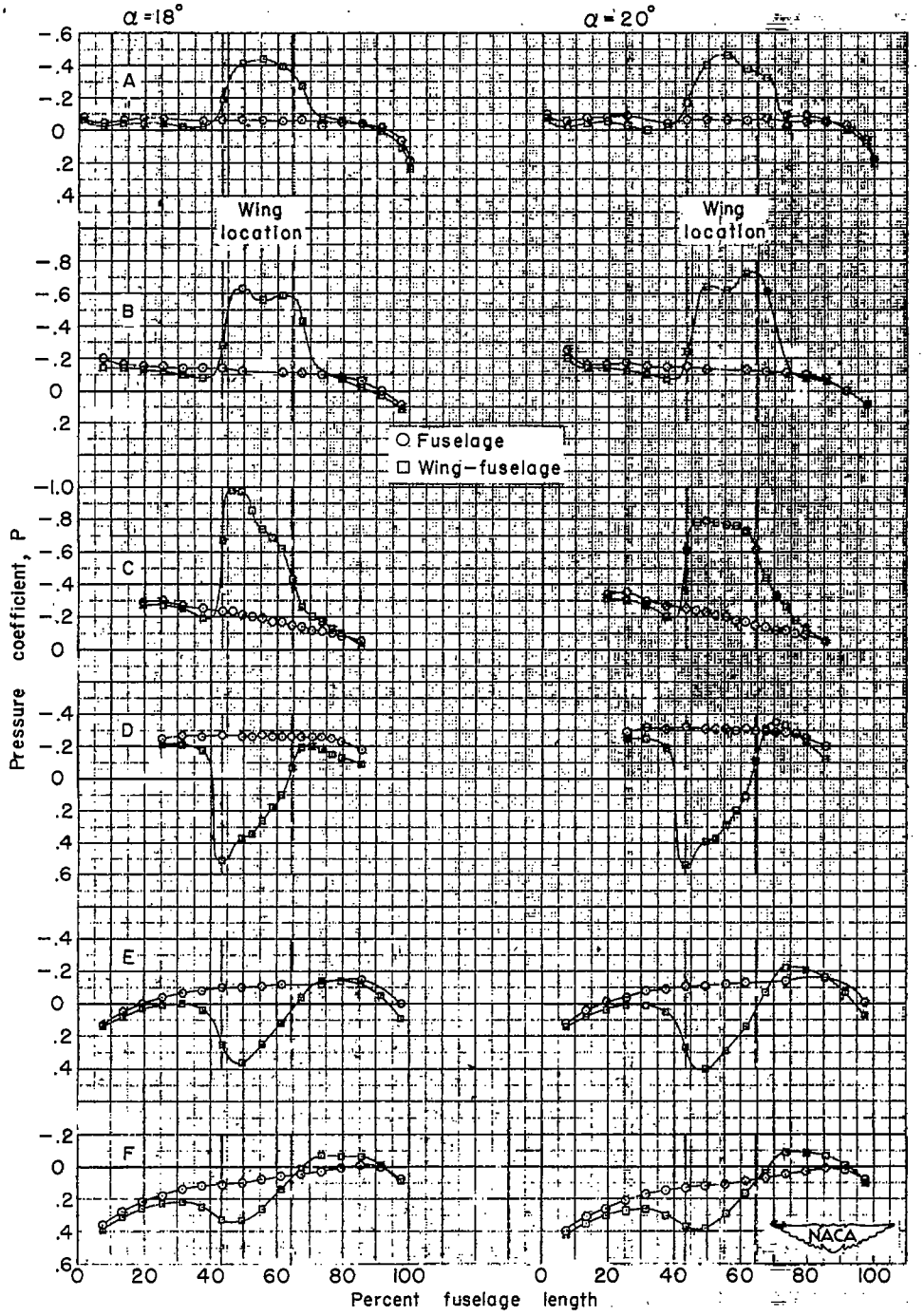

Figure 8.- The longitudinal pressure distribution at six radial locations for the fuselage and wing-fuselage configuration at several angles of attack. M = 0.79; $\alpha = 18^{\circ}$ and 20°.

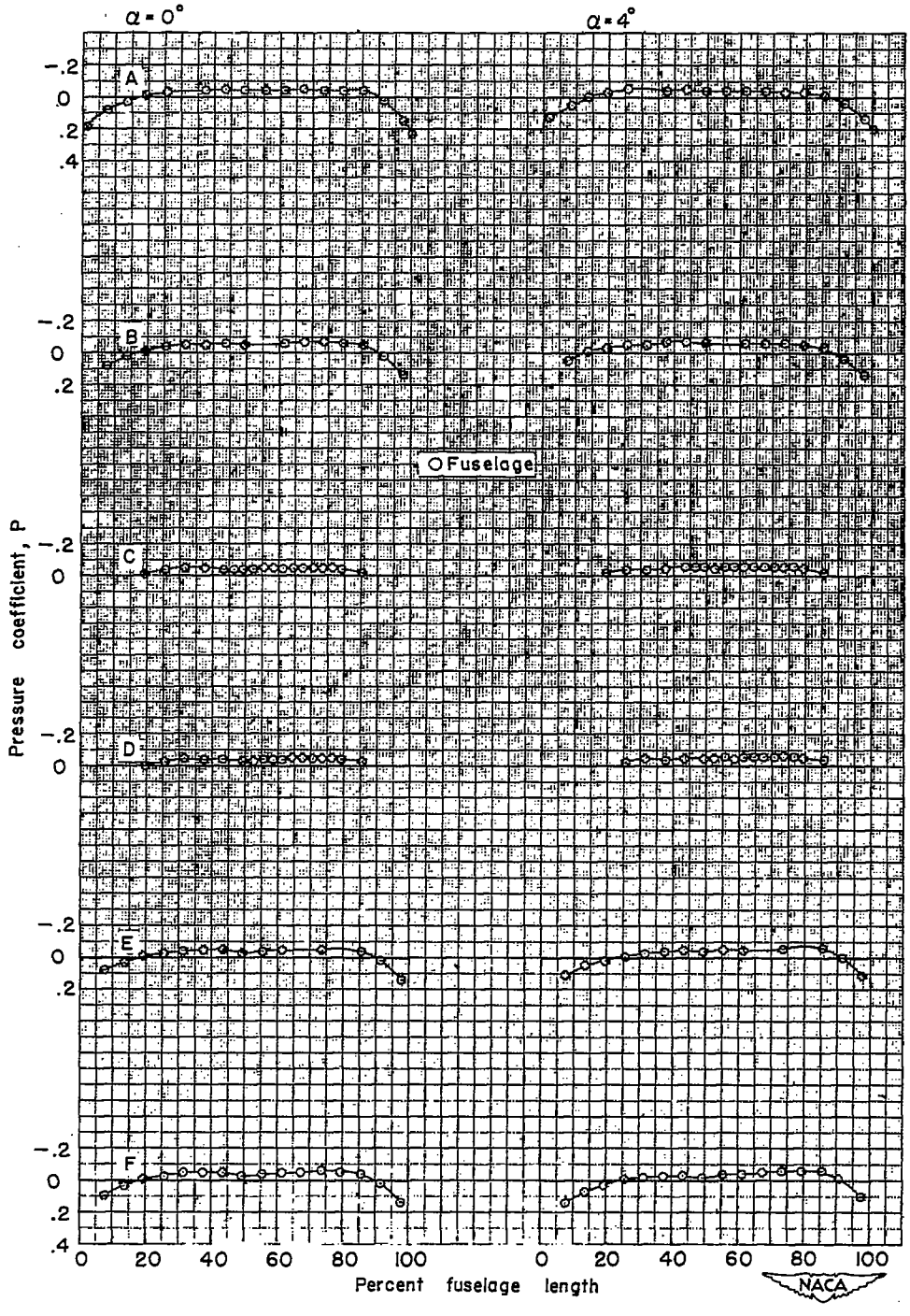

Figure 9.- The longitudinal pressure distribution at six radial locations for the fuselage configuration at various angles of attack. M = 0.89; $\alpha = 0^{\circ}$ and 4°.

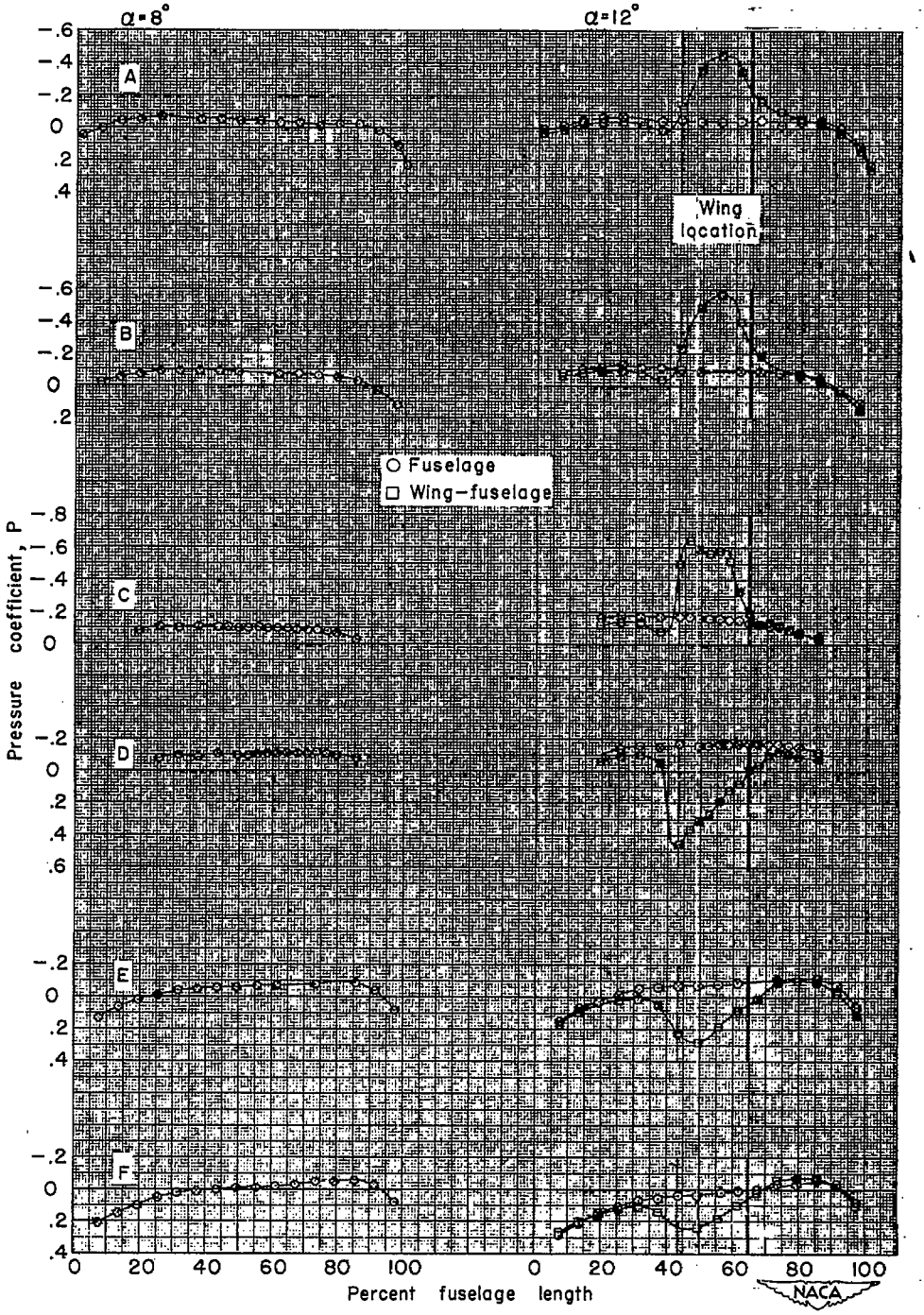

(a) M = 0.89; α = 8° and 12°.

Figure 10.- The longitudinal pressure distribution at six radial locations for the fuselage and wing-fuselage configuration at various angles of attack.

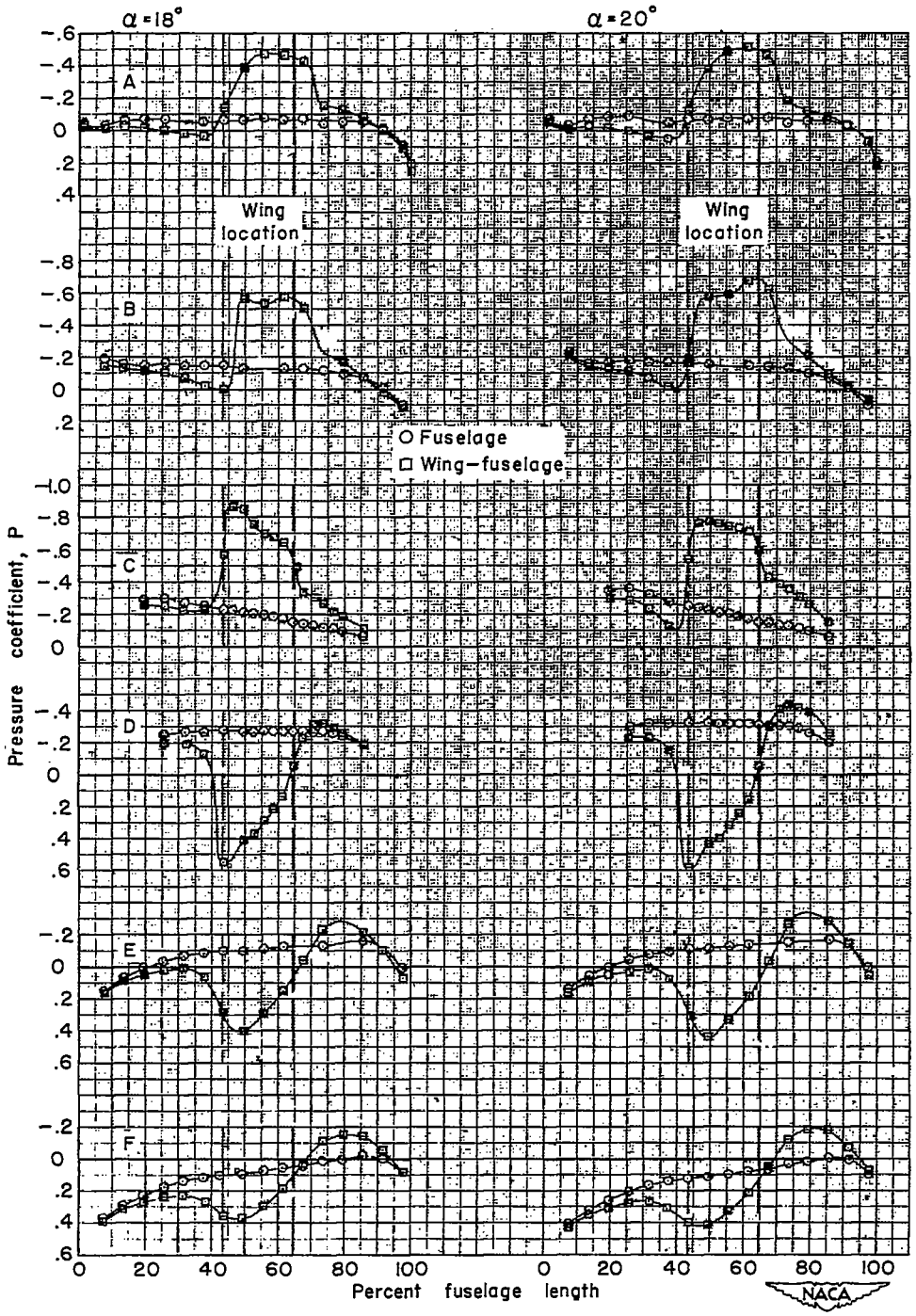

(b) M = 0.89; $\alpha = 18^{\circ}$ and 20°.

Figure 10.- Continued.

[redacted]

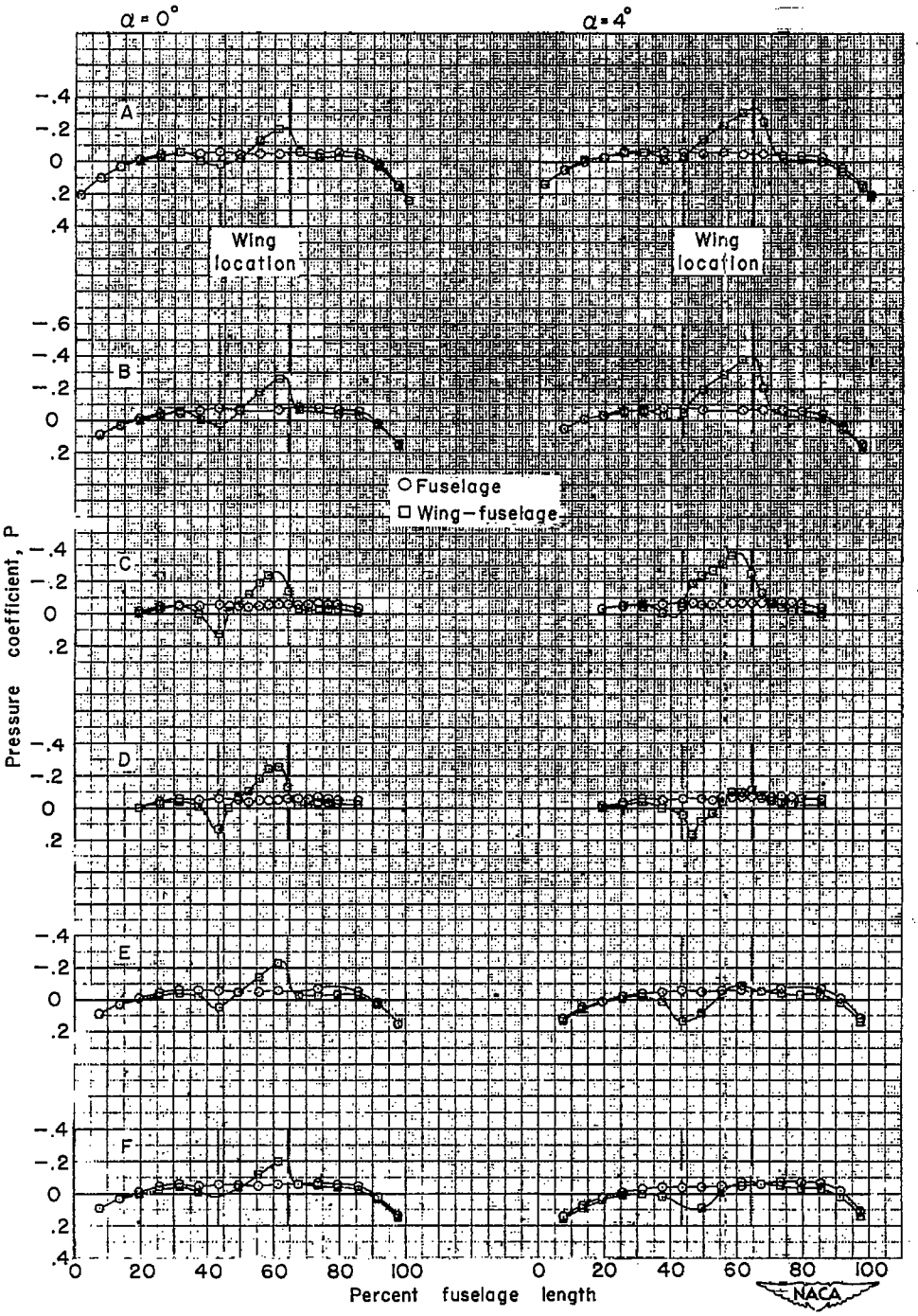

(c) M = 0.94; $\alpha = 0^{\circ}$ and 4°.

Figure 10.- Continued.

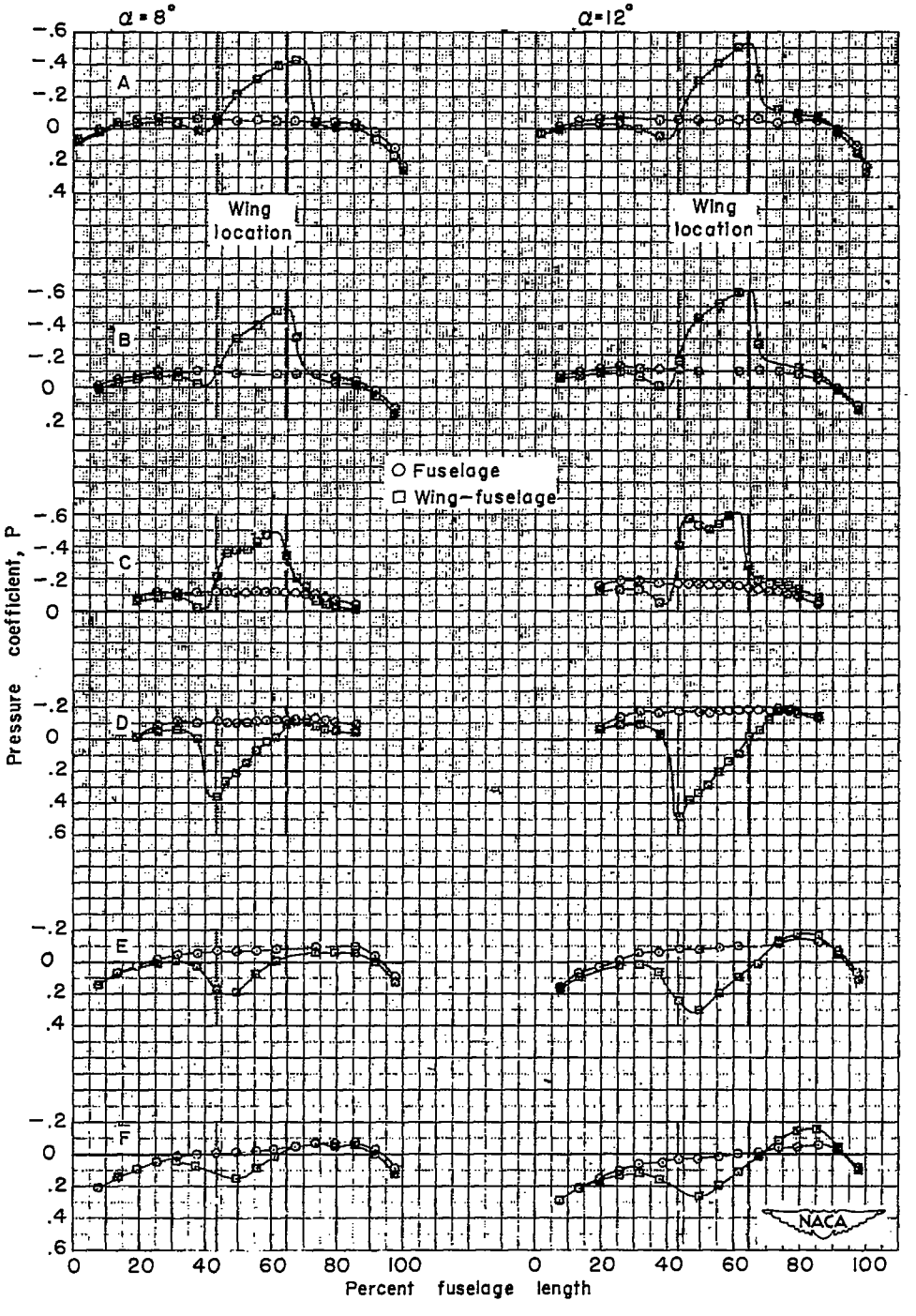

(d) M = 0.94; α = 8° and 12°.

Figure 10.- Continued.

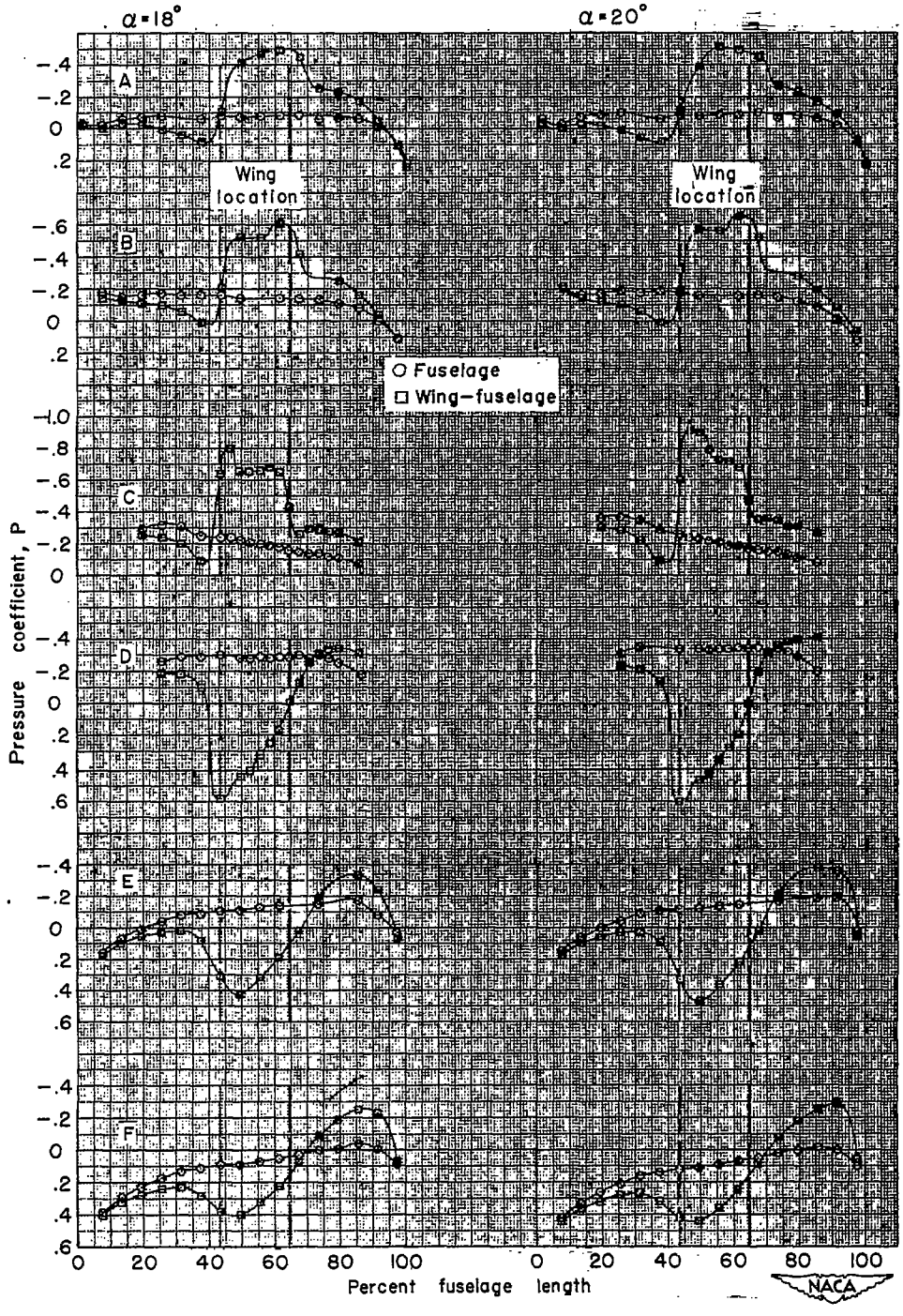

(e) M = 0.94; $\alpha = 18^{\circ}$ and 20°.

Figure 10.- Continued.

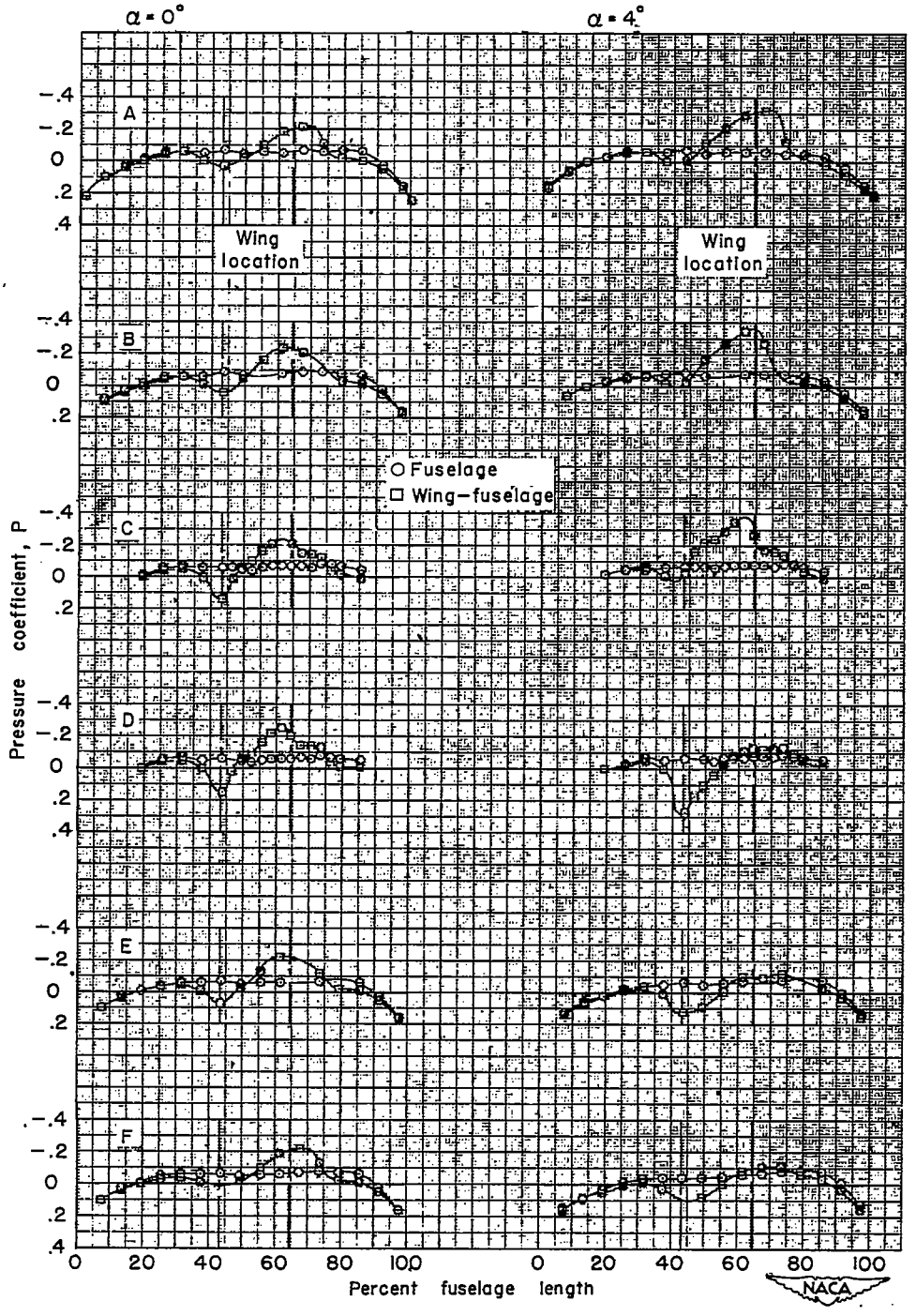

(f) M = 0.97; $\alpha = 0^\circ$ and 4°.

Figure 10.- Continued.

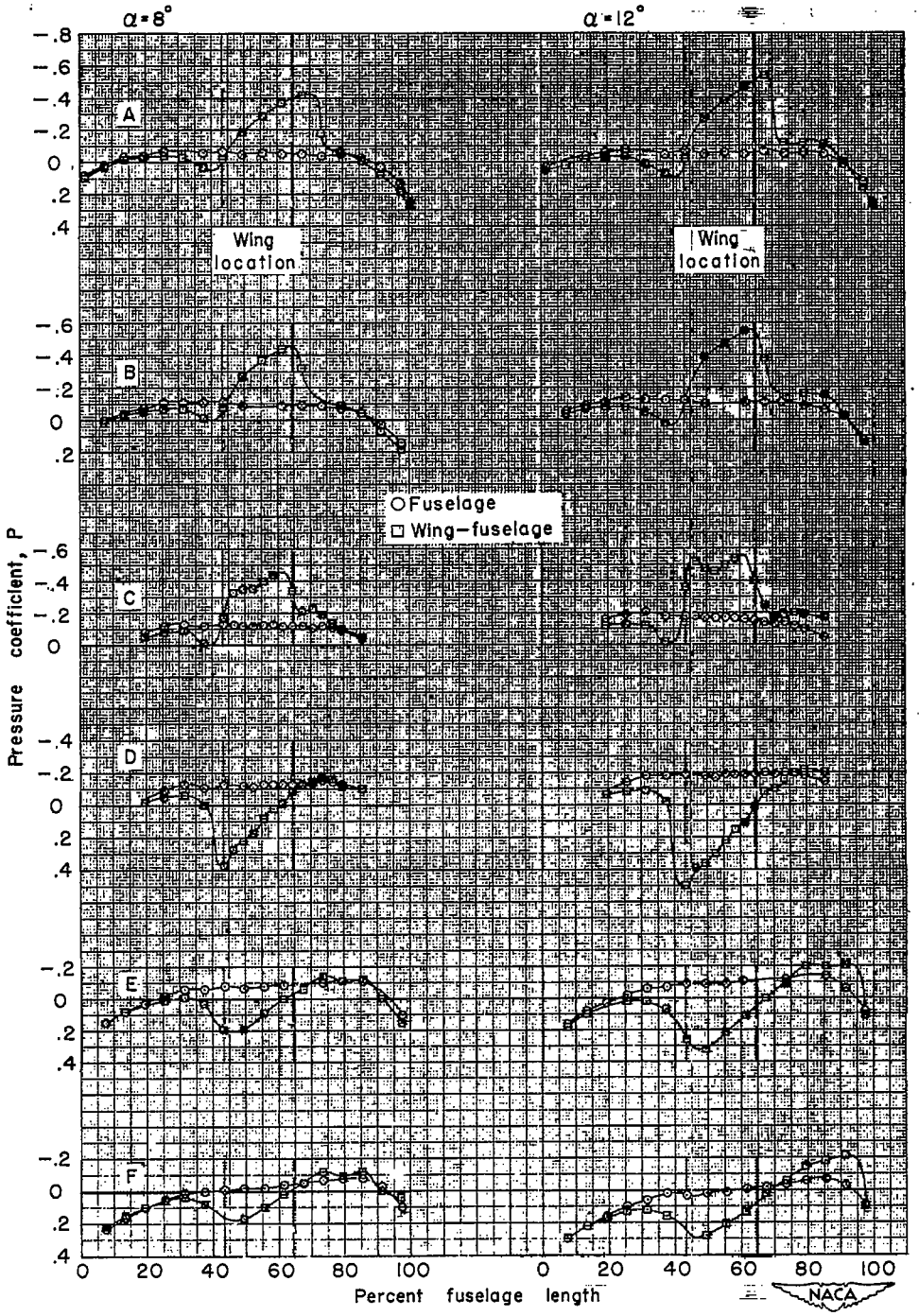

(g) M = 0.97; $\alpha = 8^{\circ}$ and 12°.

Figure 10.- Continued.

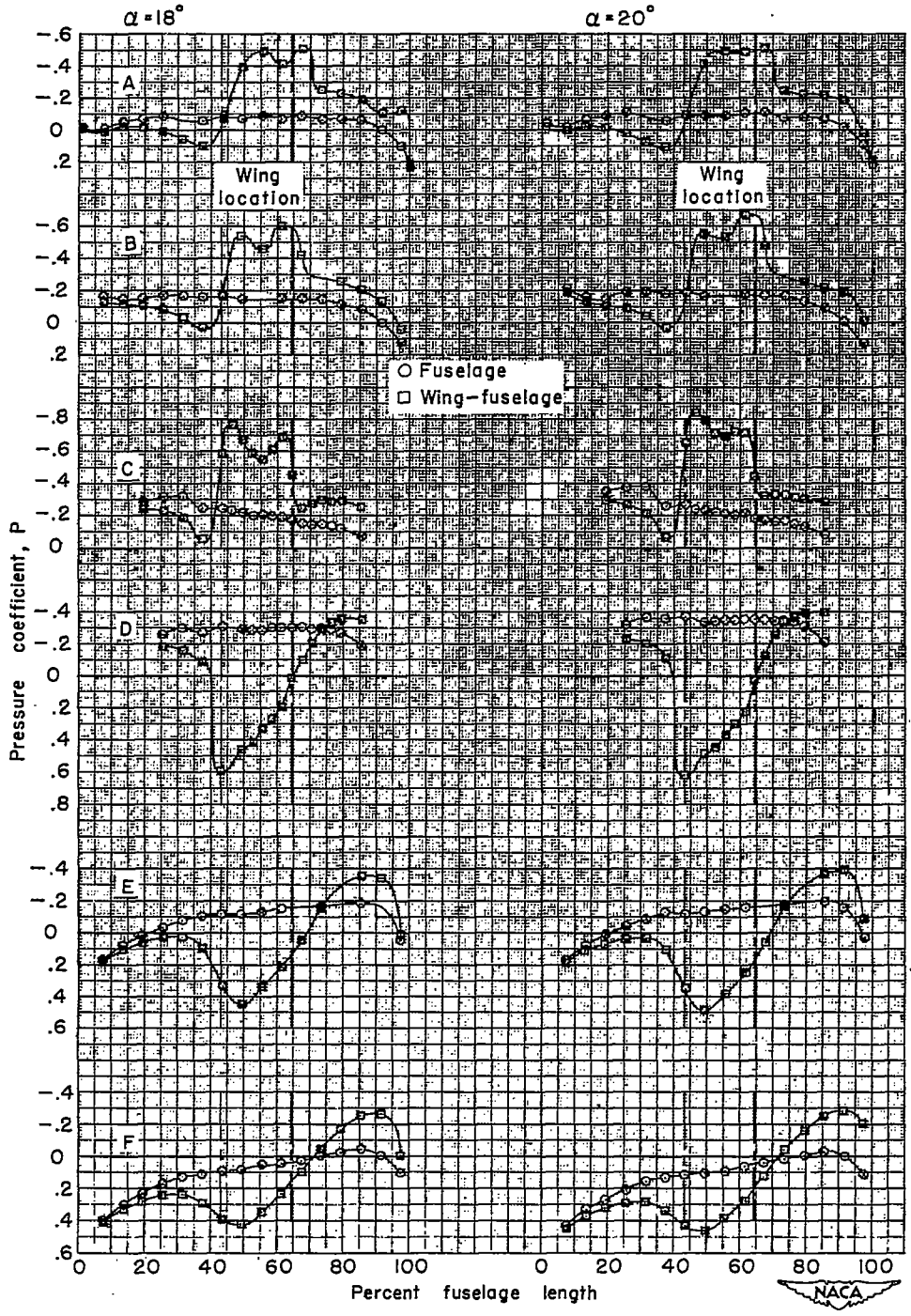

(h) M = 0.97; α = 18° and 20°.

Figure 10.- Continued.

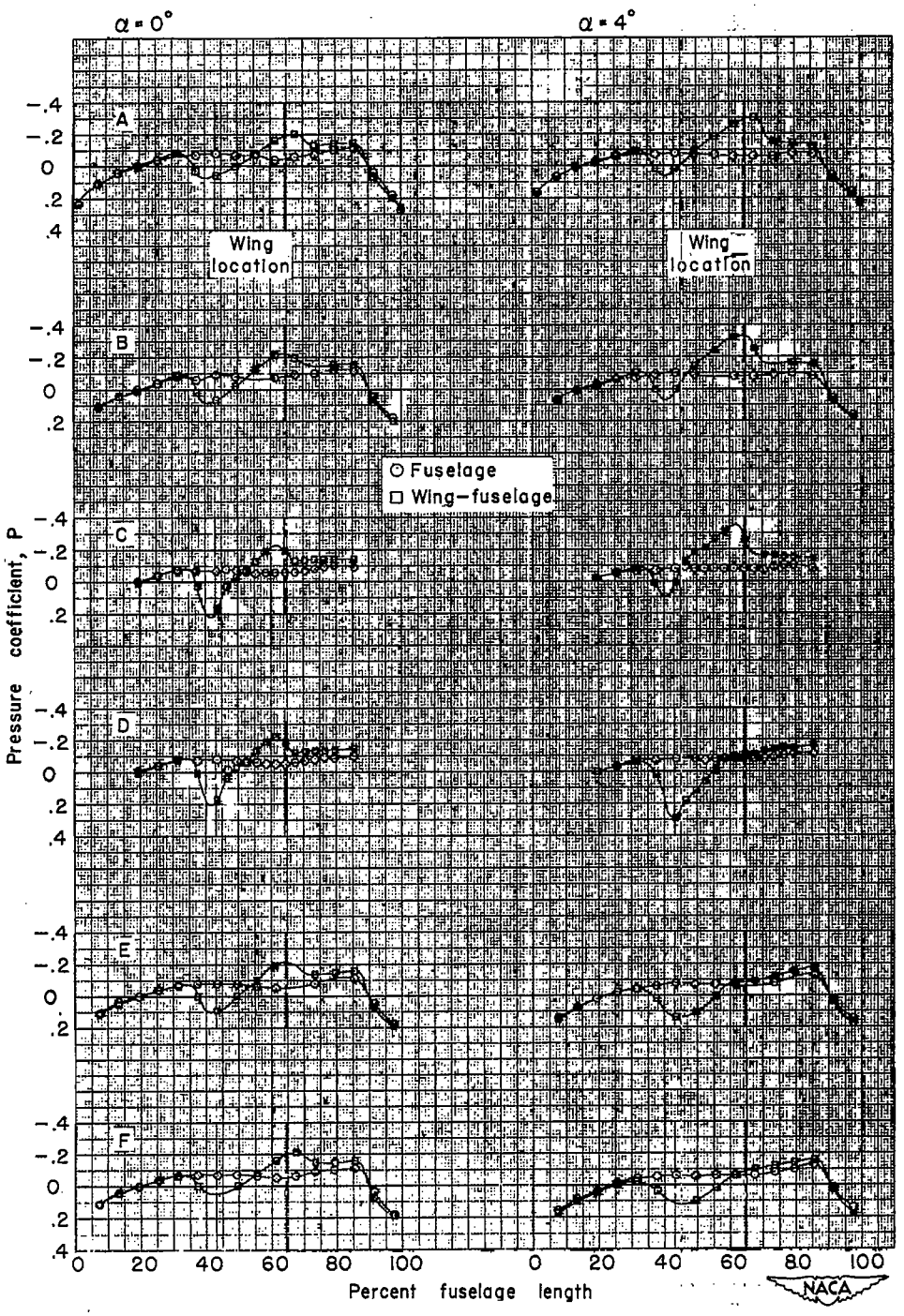

(i) M = 0.99; $\alpha = 0^\circ$ and 4°.

Figure 10.- Continued.

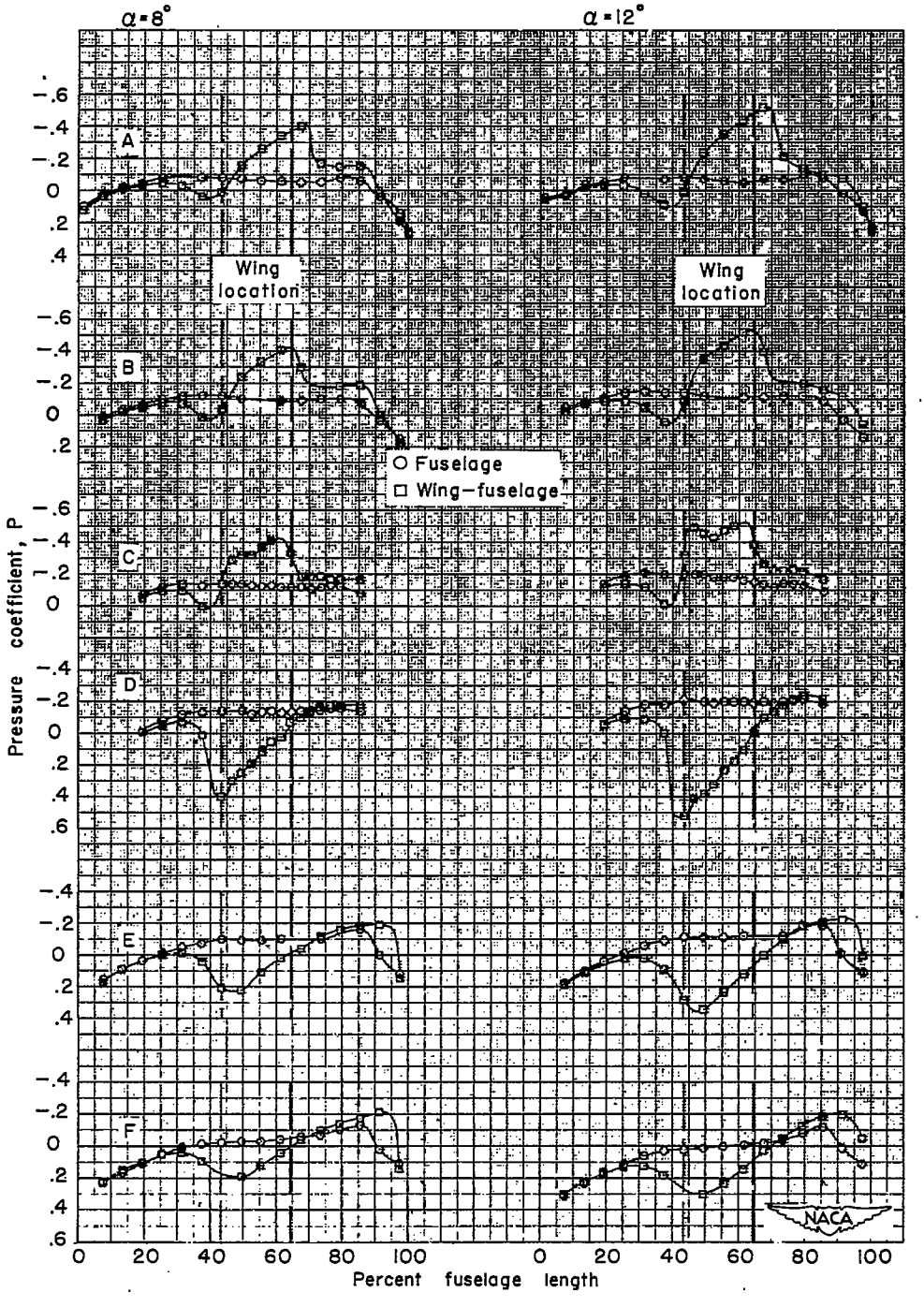

(j) M = 0.99; α = 8° and 12°.

Figure 10.- Continued.

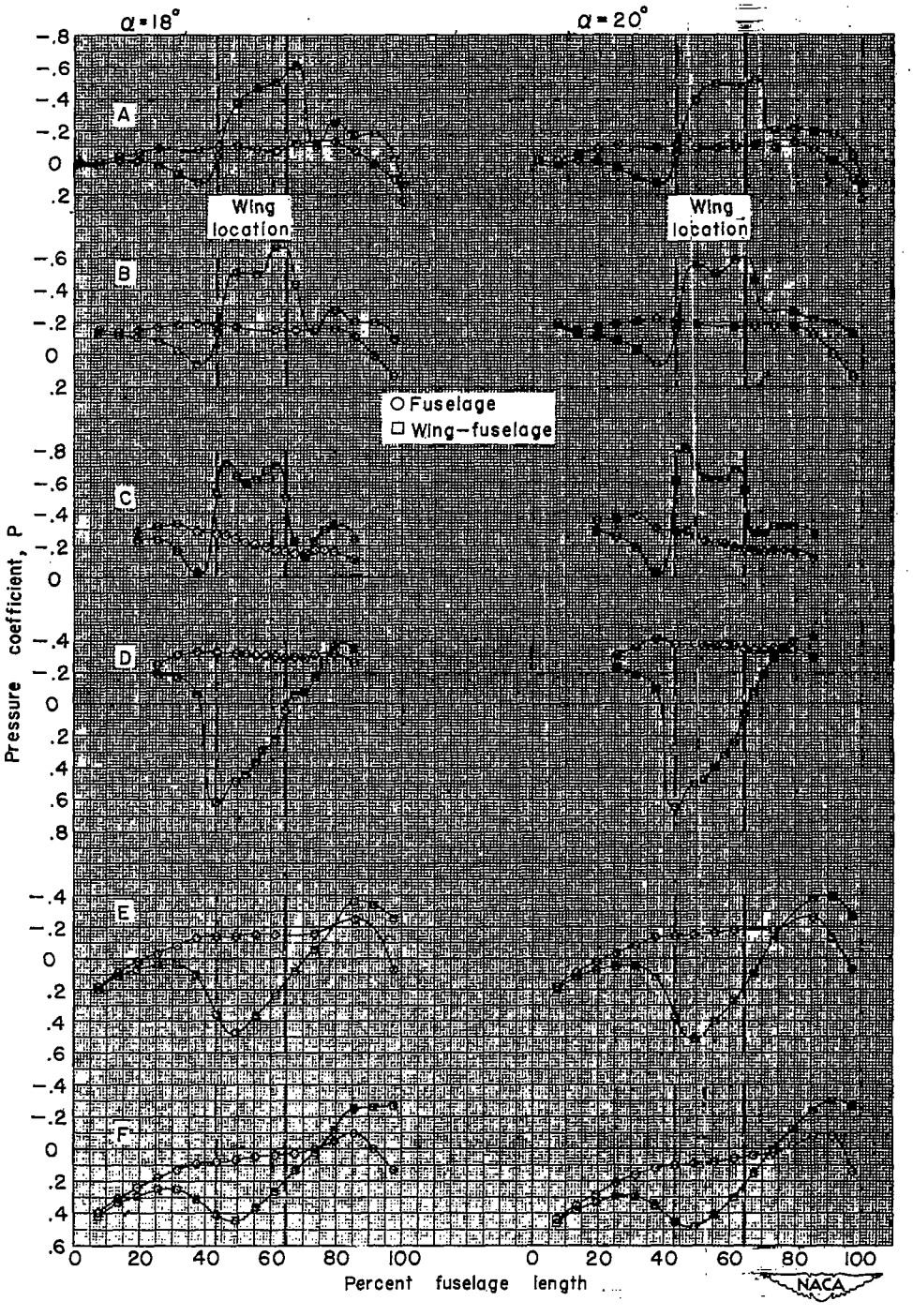

(k) M = 0.99; $\alpha = 18^\circ$ and 20°.

Figure 10.- Continued.

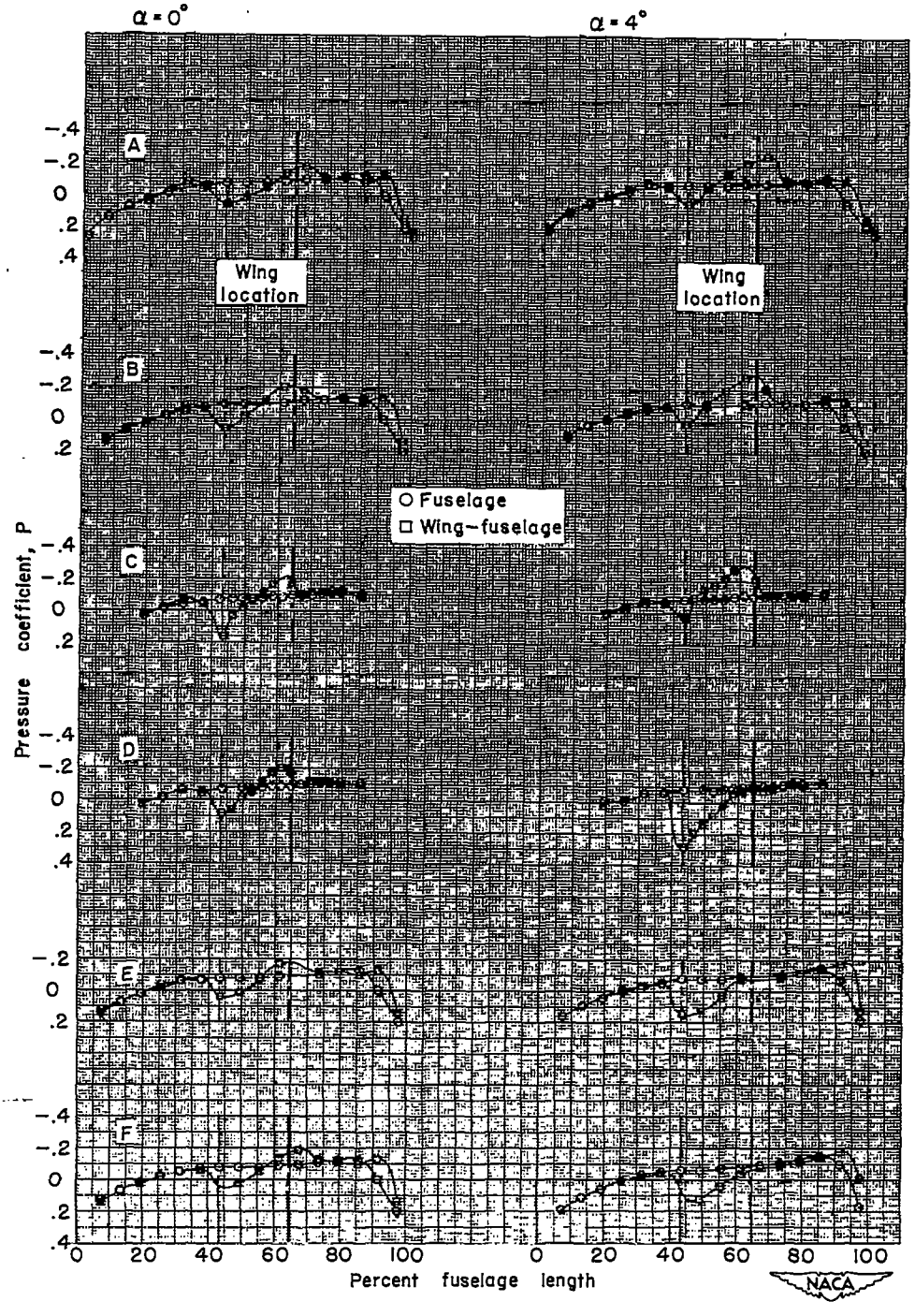

(l) M = 1.02; $\alpha = 0^\circ$ and 4°.

Figure 10.- Continued.

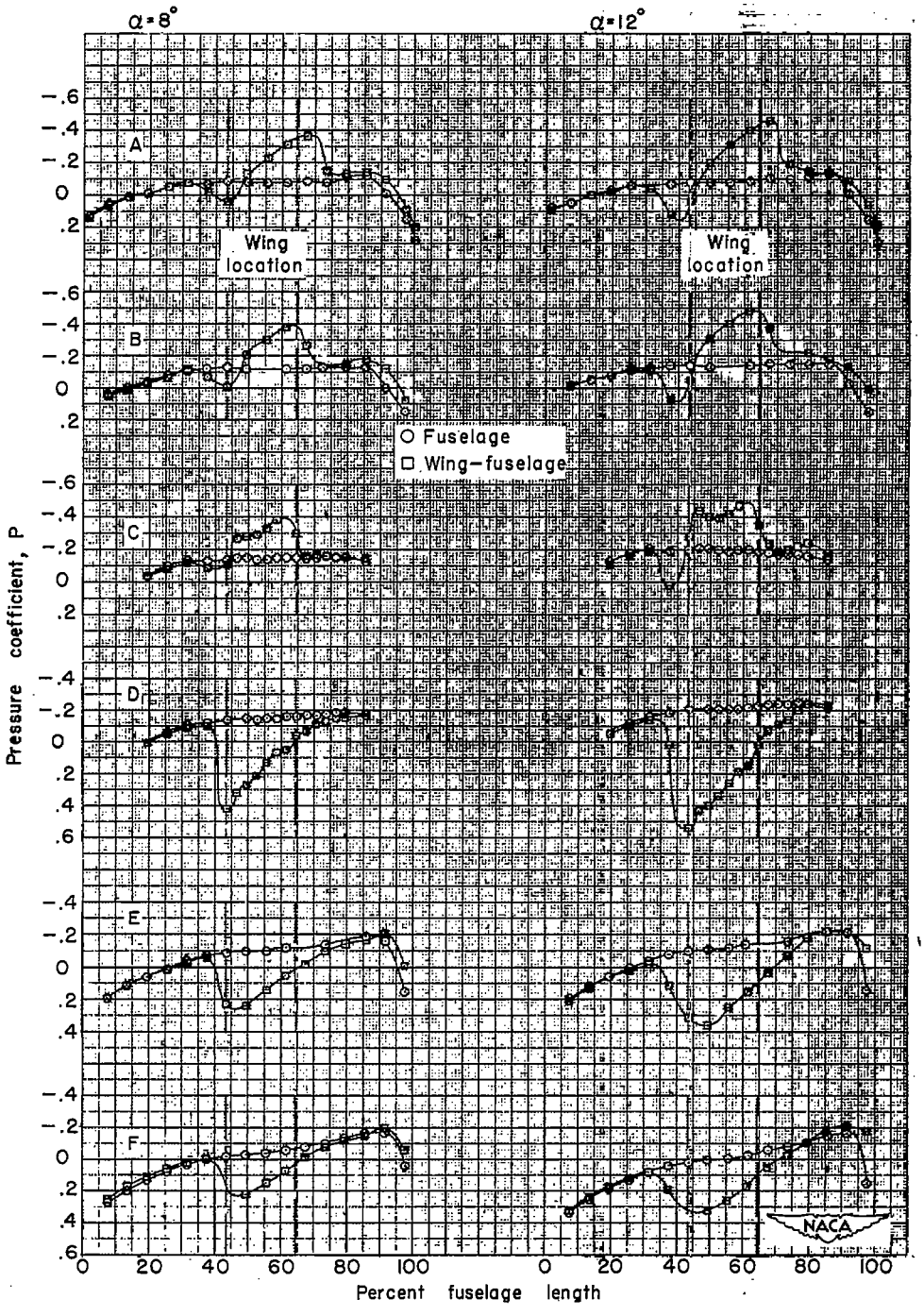

(m) M = 1.02; $\alpha = 8^{\circ}$ and 12°.

Figure 10.- Continued.

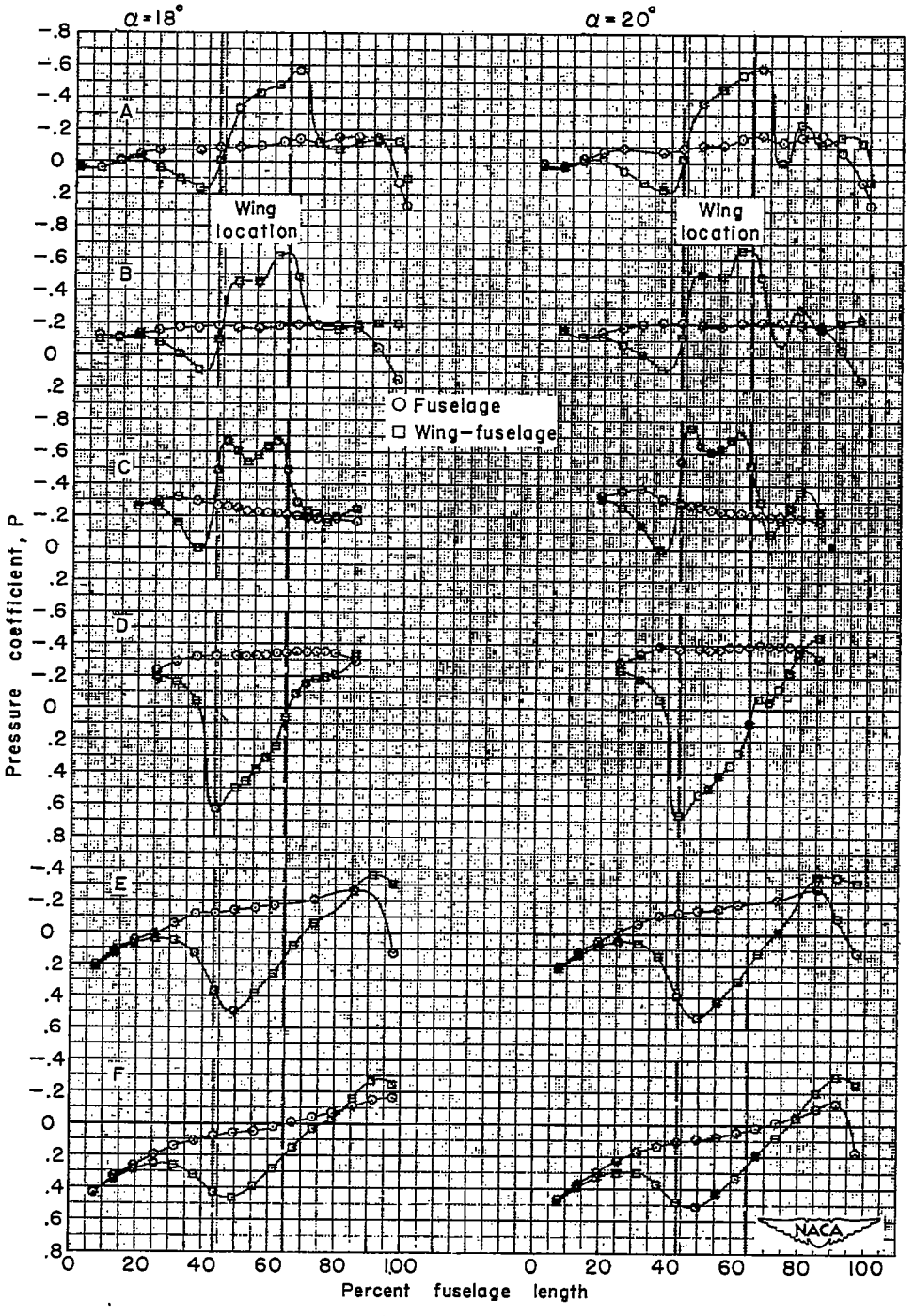

(n) M = 1.02; α = 18° and 20°.

Figure 10.- Continued.

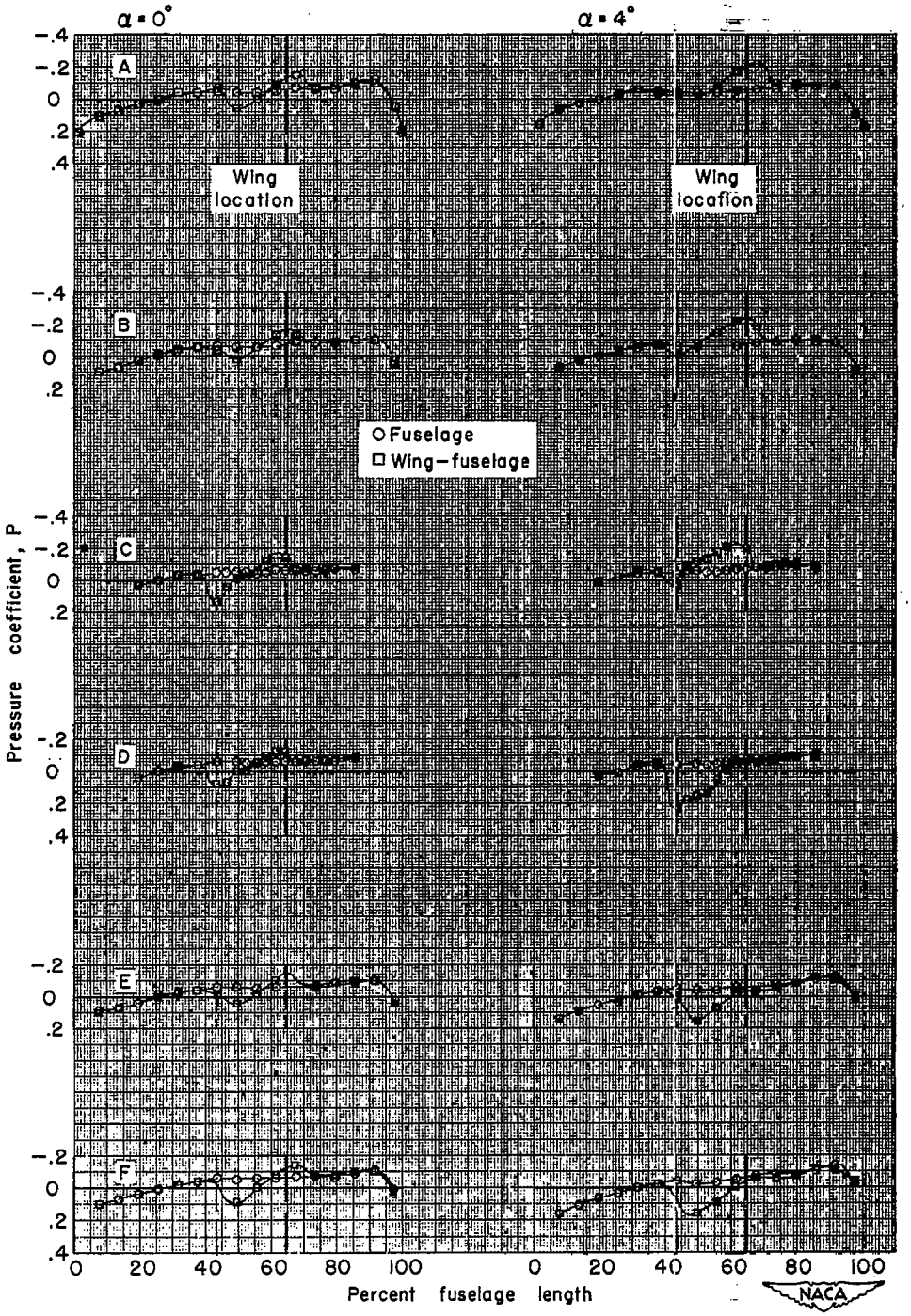

(o) M = 1.11; $\alpha = 0^\circ$ and 4°.

Figure 10.- Continued.

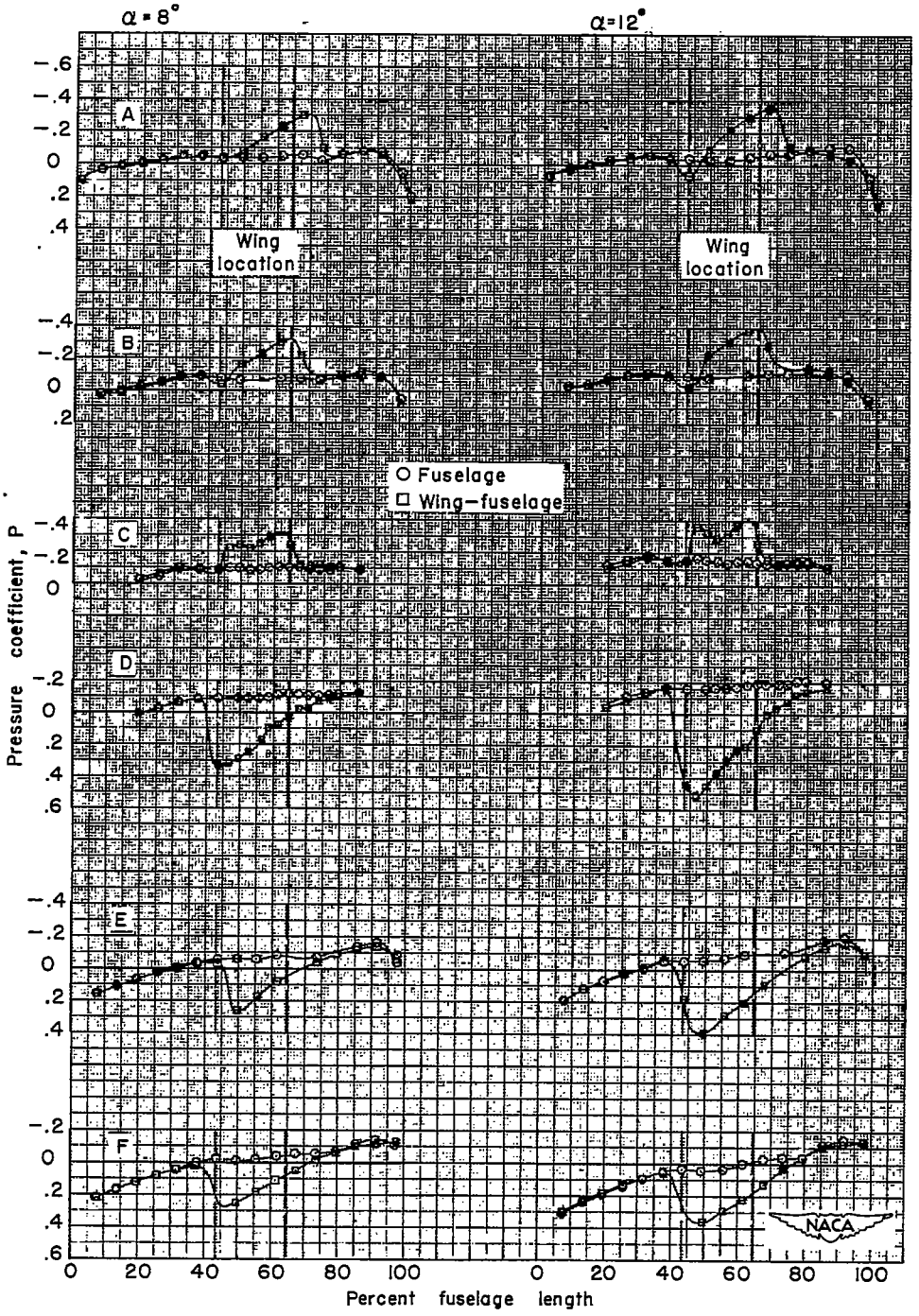

(p) M = 1.11; α = 8° and 12°.

Figure 10.- Continued.

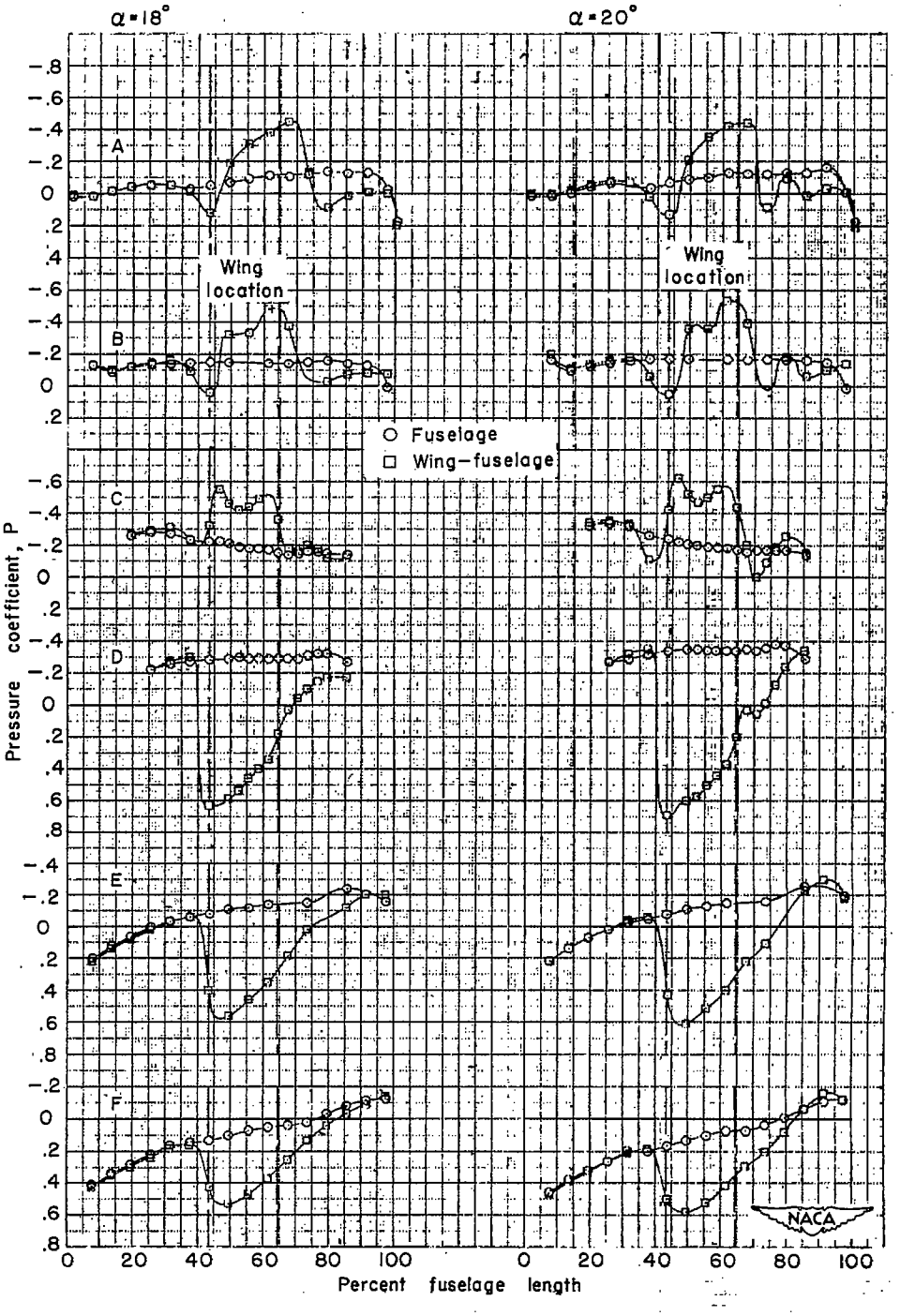

(q) M = 1.11; α = 18° and 20°.

Figure 10.- Continued.

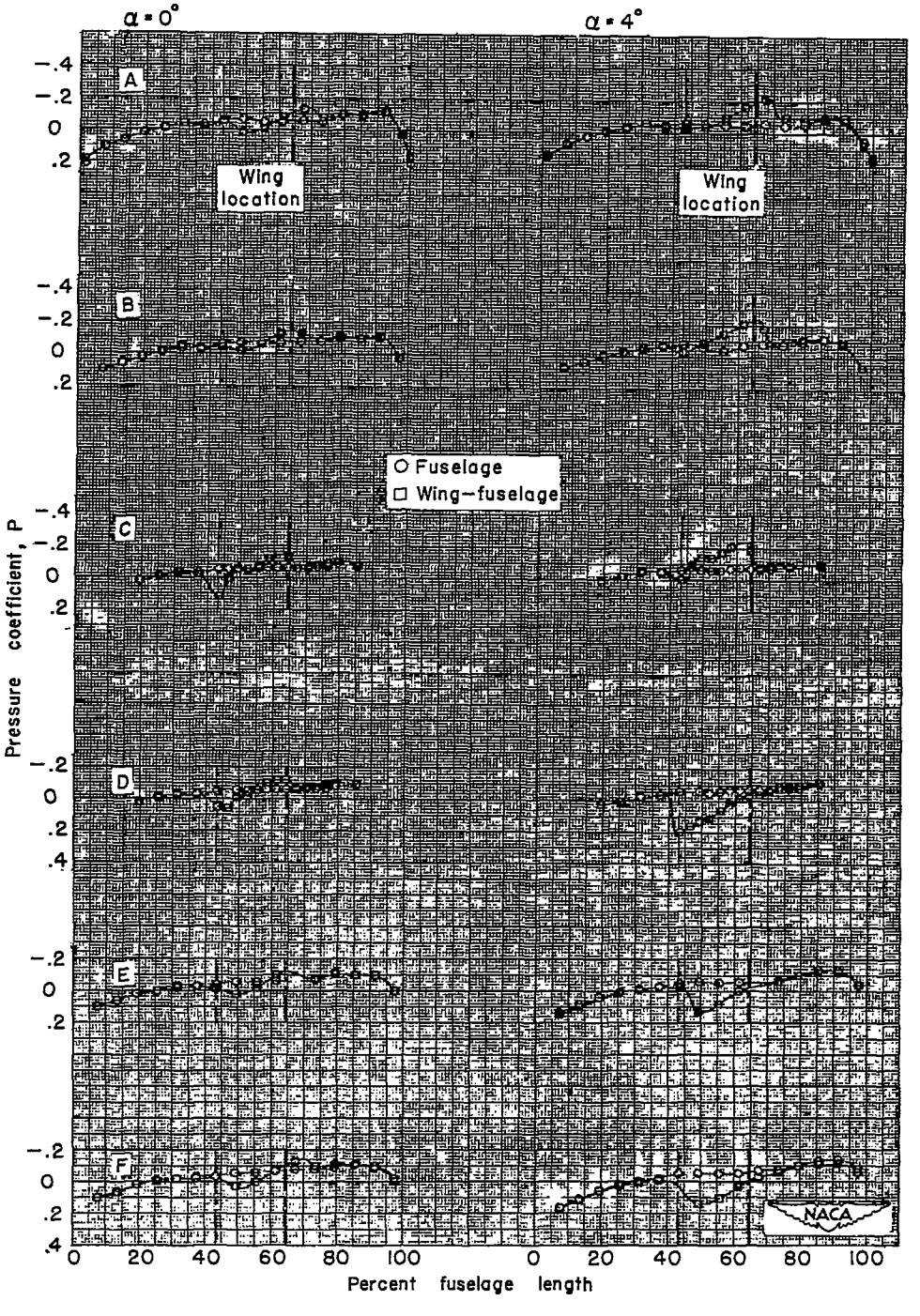

(r) M = 1.13; $\alpha = 0^{\circ}$ and 4°.

Figure 10.- Continued.

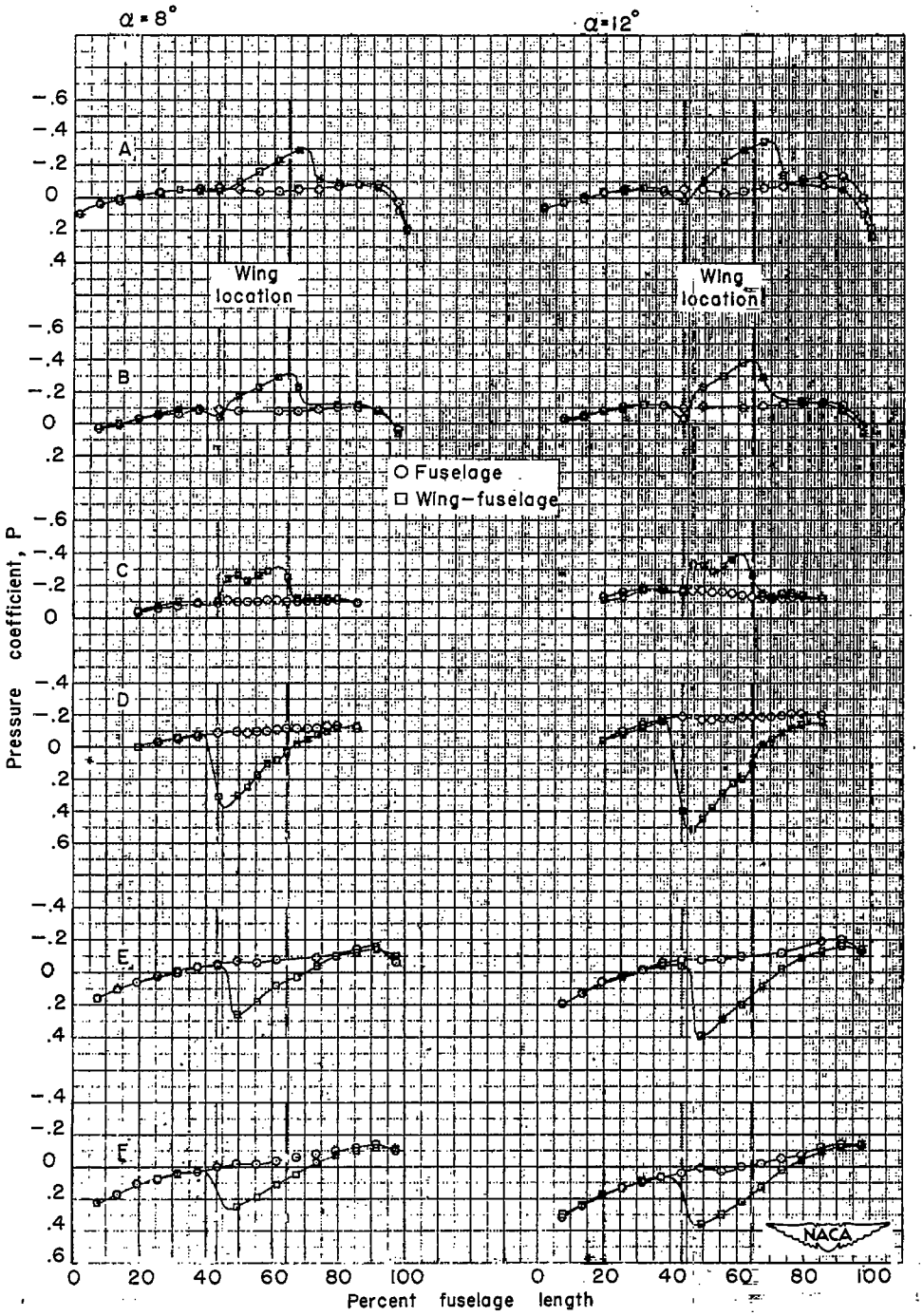

(s) M = 1.13; $\alpha = 8^\circ$ and 12° (fuselage alone).
M = 1.13; $\alpha = 8^\circ$ (wing-fuselage).
M = 1.12; $\alpha = 12^\circ$ (wing-fuselage).

Figure 10.- Continued.

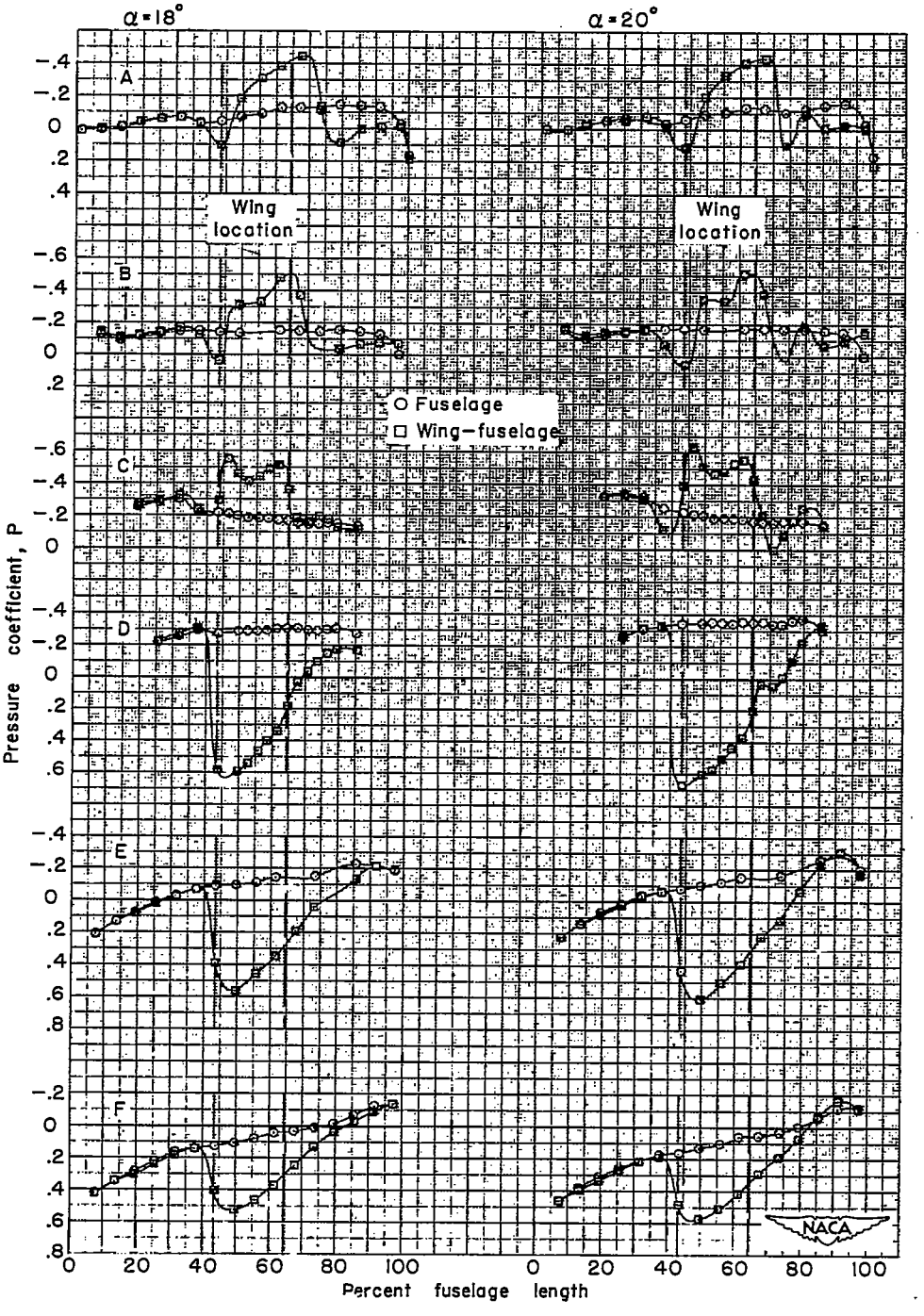

(t) M = 1.12; $\alpha = 18^{\circ}$ and 20°.

Figure 10.- Concluded.

[redacted]